

UNCLASSIFIED
CONFIDENTIAL

Copy
RM L9K11

NACA RM L9K11



445, 4
- 145-17
65-009/10
C. 2

RESEARCH MEMORANDUM

MEASUREMENTS OF AERODYNAMIC CHARACTERISTICS OF A
35° SWEPTBACK NACA 65-009 AIRFOIL MODEL WITH $\frac{1}{4}$ -CHORD
BEVELLED-TRAILING-EDGE FLAP AND TRIM TAB BY THE NACA
WING-FLOW METHOD

By Harold I. Johnson and B. Porter Brown
Langley Aeronautical Laboratory
Langley Air Force Base, Va.

CLASSIFICATION CANCELLED

CLASSIFIED DOCUMENT

Authority NACA R 7 24-83 Date 8/2/83
By SP-4A 9/7/54 See _____

This document contains classified information
under the National Defense of the United
States within the meaning of the Espionage Act,
USC 50c and 50d. The transmission or the
revelation of its contents in any manner to an
unauthorized person is prohibited by law.
Information so classified may be imparted
only to persons in the military and naval
services of the United States, appropriate
civilian officers and employees of the Federal
Government who have a legitimate interest
therein, and to United States citizens of known
loyalty and discretion who of necessity must be
informed thereof.

NATIONAL ADVISORY COMMITTEE
FOR AERONAUTICS

WASHINGTON
January 6, 1950

CONFIDENTIAL

UNCLASSIFIED



UNCLASSIFIED

NATIONAL ADVISORY COMMITTEE FOR AERONAUTICS

RESEARCH MEMORANDUM

MEASUREMENTS OF AERODYNAMIC CHARACTERISTICS OF A
35° SWEPTRACK NACA 65-009 AIRFOIL MODEL WITH $\frac{1}{4}$ -CHORD
BEVELLED-TRAILING-EDGE FLAP AND TRIM TAB BY THE NACA
WING-FLOW METHOD

By Harold I. Johnson and B. Porter Brown

S U M M A R Y

This investigation is the third of a series concerned with the determination of fundamental characteristics of trailing-edge controls at transonic speeds. A 35° sweptback untapered airfoil model of aspect ratio 3 has been fitted with various $\frac{1}{4}$ -chord full-span flaps differing only in type of aerodynamic balance. The first series of tests was run with a plain flap which represented the case of zero aerodynamic balance. The second series of tests was run with a flap that had a large horn balance. Results from these two series of tests have been reported previously. The tests described herein were made with a flap that incorporated a bevelled trailing edge with an included trailing-edge angle of 23°. Important results follow.

The lift characteristics of the model and flap were similar to those measured previously with true-contour flaps on the model. Sealing the flap gap increased the lift-curve slope and the flap effectiveness appreciably and also caused a rearward shift in the center of pressure of the load due to flap deflection. The $\frac{1}{3}$ -flap-chord by $\frac{1}{3}$ -flap-span bevelled trim tab had poor trimming characteristics at all speeds tested ($M = 0.65$ to 1.15), inasmuch as the hinge moment due to tab deflection reversed for various parts of the deflection range at different Mach numbers. The bevelled trailing edge appears to be an unsatisfactory type of aerodynamic balance for airplanes required to traverse a large speed range because at subsonic speeds the degree of balance was highly nonuniform and at low supersonic speeds most of the balancing effectiveness disappeared.

~~CONFIDENTIAL~~

UNCLASSIFIED

I N T R O D U C T I O N

A wing-flow investigation is being made to determine the characteristics of conventional low-speed aerodynamic balances at transonic speeds. In this investigation a typical sweptback airfoil-flap combination representing either a wing or a tail surface is being fitted with $\frac{1}{4}$ -chord full-span flaps differing only in type of aerodynamic balance. The primary objectives of the investigation are the determination of flap hinge moments and flap effectiveness; however, it has been found convenient and desirable also to measure the lift and pitching-moment characteristics of the complete models. The first series of tests was made with a plain flap which represents the case of zero aerodynamic balance (reference 1). The second series of tests was made with a horn-balanced flap that was designed to have a large degree of aerodynamic balance at low speeds (reference 2). The present series of tests was made with a bevelled-trailing-edge flap that had a trailing-edge angle of 23° in planes perpendicular to the hinge line. The true-contour NACA 65-009 section flap tested in reference 1 had a trailing-edge angle of approximately 6° .

The tests consisted of measurements of the lift, pitching moments, and hinge moments acting on a semispan airfoil-flap model having a sweepback angle of 35° , an aspect ratio of 3.07, a taper ratio of 1.0, an NACA 65-009 section in planes perpendicular to the leading edge over the forward 75 percent of the chord, a full-span $\frac{1}{4}$ -chord bevelled-trailing-edge flap, and a $\frac{1}{3}$ -span by $\frac{1}{3}$ -flap-chord trim tab. Tests were made with the flap gap both sealed and unsealed. In general, data were obtained over an angle-of-attack range of -5° to 18° , a flap-deflection range of $\pm 20^\circ$, a tab-deflection range of 0 to 10° , a Mach number range of 0.55 to 1.15, and a Reynolds number range of about 500,000 to 1,400,000. Because the tests were run within two widely separated altitude ranges, the data can be used to study some effects of Reynolds number even though the highest Reynolds number encountered was small in comparison with probable full-scale Reynolds numbers.

S Y M B O L S

M	average Mach number over model
M_A	airplane free-stream Mach number
R	Reynolds number

q_A	airplane free-stream dynamic pressure
q	average dynamic pressure over model
C_{L_A}	airplane lift coefficient $\left(\frac{\text{Airplane lift}}{q_A S_A} \right)$
C_L	model lift coefficient $\left(\frac{\text{Model lift}}{q S} \right)$
C_m	model pitching-moment coefficient (measured about axis 18.1 percent M.A.C. ahead of leading edge of M.A.C.) $\left(\frac{\text{Model pitching moment}}{q b \bar{c}^2} \right)$
C_h	model hinge-moment coefficient $\left(\frac{\text{Model hinge moment}}{q b_f \bar{c}_f^2} \right)$
C_{L_α}	variation of model lift coefficient with angle of attack, per degree $\left(\frac{\partial C_L}{\partial \alpha} \right)$
C_{L_δ}	variation of model lift coefficient with flap deflection, per degree $\left(\frac{\partial C_L}{\partial \delta_f} \right)$
C_{m_α}	variation of model pitching-moment coefficient with angle of attack, per degree $\left(\frac{\partial C_m}{\partial \alpha} \right)$
C_{m_δ}	variation of model pitching-moment coefficient with flap deflection, per degree $\left(\frac{\partial C_m}{\partial \delta_f} \right)$
C_{h_α}	variation of flap hinge-moment coefficient with model angle of attack, per degree $\left(\frac{\partial C_h}{\partial \alpha} \right)$
C_{h_δ}	variation of flap hinge-moment coefficient with flap deflection, per degree $\left(\frac{\partial C_h}{\partial \delta_f} \right)$
$\frac{\partial \alpha}{\partial \delta}$	flap relative effectiveness $\left(\frac{\partial C_L / \partial \delta_f}{\partial C_L / \partial \alpha} \right)$

α	angle of attack between model chord plane and direction of relative wind
δ_f	flap deflection angle between flap chord line and airfoil chord line measured in plane perpendicular to hinge line
δ_{TT}	trim-tab deflection in plane perpendicular to hinge line
Λ	sweepback angle
λ	taper ratio
A	aspect ratio
b	model span normal to wind direction (corresponds to one-half of span of complete wing)
c	model chord parallel to wind direction
\bar{c}	model mean aerodynamic chord (M.A.C.)
S	total area of model (corresponds to one-half of area of complete wing)
b_f	flap span along hinge line (corresponds to one-half of span of full-span flap on complete wing)
\bar{c}_f	flap root-mean-square chord perpendicular to hinge line
c_f	flap chord parallel to wind direction
S_f	flap area rear of hinge line
ϕ	included trailing-edge angle of flap
b_{TT}	trim-tab span parallel to hinge line
\bar{c}_{TT}	trim-tab chord normal to hinge line
S_{TT}	trim-tab area
S_A	airplane wing area

A P P A R A T U S

The model was mounted on the upper surface of an F-51D airplane wing as shown in figure 1. The wing contour had been modified to provide more uniform velocity gradients over the model test station. Typical local velocity gradients in both the chordwise and spanwise directions over the model test station are shown in figures 2 and 3, respectively. In calculating force and moment coefficients, an average dynamic pressure corresponding to the average local Mach number over the model area was used. No correction was applied for the effect of the wing boundary layer. Other tests have shown that the wing boundary layer has a total thickness of only about $1/4$ inch. The effect of the wing boundary layer on the velocity distribution over the model, therefore, was considered to be negligible. The effects of model flexibility were small and also considered to be negligible. Flexibility effects are discussed in more detail in reference 1.

A drawing of the bevelled-trailing-edge flap model including a list of pertinent dimensions is given in figure 4. The model was intended to have exactly the same over-all dimensions as those tested in references 1 and 2; however, small errors were made in the construction of the flap so that the model aspect ratio was changed from 3.04 to 3.07 and the flap-chord ratio was changed from 0.25 to 0.24. The model was machined from solid duralumin and an end plate of diameter equal to the chord was attached at the root of the model. The gap between the flap leading edge and the basic airfoil model was approximately 0.015 inch (0.005c). In tests of the sealed-gap condition the gap was closed along 64 percent of the flap span by 0.002-inch-thick sheet rubber installed as shown in figures 4 and 5.

The bevelled-trailing-edge flap had an included trailing-edge angle of 23° in planes perpendicular to the hinge line as compared with a trailing-edge angle of about 6° for the true-contour NACA 65-009 section tested in reference 1. In the streamwise direction the trailing-edge angle was 19.2° . The bevelled portion of the flap extended forward from the trailing edge about one-fourth of the flap chord. From this point to the hinge line the surface was formed by a plane tangent to the flap-nose radius, which was the standard nose radius for a 25-percent-chord flap on an NACA 65-009 section. (See figs. 4 and 5.) The flap had a $\frac{1}{3}$ -span by $\frac{1}{3}$ -chord tab, located centrally along the span, which could be bent to desired deflections. Bending of the tab was facilitated by cutting U-shaped grooves in the flap at the tab leading edge along the entire tab span. The tab gap was, therefore, completely sealed for all tests.

The recording instrumentation was the same as that described in references 1 and 2.

T E S T S

The data presented were obtained from nine flights. Of these nine flights, two were made to obtain model and flap characteristics with flap gap open (gap = 0.0058), four were made to obtain model and flap characteristics with the flap gap sealed along 64 percent of the span, and three were made to obtain trim-tab-effectiveness data with the flap gap sealed.

With gap open, one flight was made with the flap fixed in neutral and the entire model oscillating through an angle-of-attack range of -5° to 18° . The other flight was made with the model fixed at zero angle of attack relative to the airplane X-axis and the flap oscillating through a deflection range of about $\pm 20^{\circ}$. This procedure was repeated for the gap-sealed condition; however, an additional two flights were made with gap sealed in which the model was fixed at $\alpha = 5^{\circ}$ and $\delta_f = 5^{\circ}$, successively. In all the foregoing flights the trim tab was set in neutral. Trim-tab data were obtained by fixing the model at $\alpha \approx 0^{\circ}$, oscillating the flap through a deflection range of $\pm 20^{\circ}$, and setting the trim tab on successive flights to deflections of 1.95° , 5.4° , and 10.8° . The rate of oscillation of either the model or the flap was approximately one cycle per second.

Each flight was made up of two test runs referred to hereinafter as the "high-dive" run and the "level-flight" run. (Trim-tab characteristics were measured only in high-dive runs.) The high-dive run was made by diving the airplane from 28,000 feet and an indicated airspeed of 220 miles per hour to an airplane Mach number of 0.73 at approximately 18,000 feet. During this run usable data were obtained for average Mach numbers over the model ranging from 0.65 to 1.15 at relatively lower Reynolds numbers. The level-flight run was made by gradually slowing the airplane from 450 miles per hour to 300 miles per hour at 5,000 feet altitude following a dive and pull-out from about 15,000 feet altitude. During this run usable data were obtained for average Mach numbers over the model ranging from 0.55 to 0.95 (sometimes 1.0) at relatively higher Reynolds numbers. Typical variations of Reynolds number with Mach number for the two types of test runs are given in figure 6.

A C C U R A C Y

The accuracy of the major variables in this investigation was estimated to be as follows:

Mach number	±0.01
Angle of attack, degree	±0.3
Flap angle, degree	±0.3
Trim-tab angle, degree	±0.1
Lift coefficient	±0.03
Pitching-moment coefficient	±0.015
Hinge-moment coefficient	±0.003

Accuracies of the last three variables listed are given for the lowest test speed; at the highest test speed, these accuracies should be approximately four times better. A large part of the loss in accuracy was attributable to shifts in instrument zeros that occurred gradually during a flight. Hence, the errors in the data appear for the most part as errors in angles of zero lift, angles of zero pitching moment, and angles of zero hinge moment. Because the data at any given Mach number were obtained within a very short period of time (less than 1 sec), the slopes of the various force- and moment-coefficient curves should be accurate to a degree approaching the instrument capabilities, which, in the present case, add up to about 2 percent at intermediate test speeds.

P R E S E N T A T I O N O F D A T A

All force and moment coefficients are presented in accordance with standard NACA conventions regarding definitions and signs. Pitching moments were measured about an axis located 18.1 percent chord forward of the leading edge of the mean aerodynamic chord.

In accordance with past procedure (see reference 2) all the basic data are presented without showing test points. However, in order to show the quality of the data, two typical plots of basic data are shown in figure 7. These plots show the number of test points evaluated at each Mach number from the continuous records of force, moment, and position.

The following tables give the order of treatment of the results as well as a key to figures 8 to 30. In general, each figure consists of two parts. The first part shows data from the high-dive runs (higher maximum Mach number, lower Reynolds numbers) and the second part shows data from the level-flight runs (higher Reynolds numbers, lower

maximum Mach number). The basic data are generally given for Mach number increments of 0.05 through the Mach number range tested.

BASIC DATA

Characteristics	Content	Gap	Figure
Lift	C_L against α ($\delta_F = 0^\circ$)	Open and sealed	8
	C_L against α ($\delta_F = 5^\circ$)	Sealed	9
	C_L against δ_F ($\alpha \approx 0^\circ$)	Open and sealed	10
	C_L against δ_F ($\alpha \approx 5^\circ$)	Sealed	11
Pitching moment	C_m against α ($\delta_F = 0^\circ$)	Open and sealed	12
	C_m against α ($\delta_F = 5^\circ$)	Sealed	13
	C_m against δ_F ($\alpha \approx 0^\circ$)	Open and sealed	14
	C_m against δ_F ($\alpha \approx 5^\circ$)	Sealed	15
Hinge moment	C_h against α ($\delta_F = 0^\circ$)	Open and sealed	16
	C_h against α ($\delta_F = 5^\circ$)	Sealed	17
	C_h against δ_F ($\alpha \approx 0^\circ$)	Open and sealed	18
	C_h against δ_F ($\alpha \approx 5^\circ$)	Sealed	19
	C_h against δ_F ($\alpha \approx 0^\circ$; $\delta_{TT} = 0^\circ, 1.95^\circ,$ $5.4^\circ, \text{ and } 10.8^\circ$)	Sealed	20

SUMMARY DATA

Characteristics	Content	Gap	Figure
Lift	$CL_\alpha, CL_\delta, \frac{\partial \alpha}{\partial \delta_f}$ against M ($\alpha \approx 0^\circ; \delta_f = 0^\circ$)	Open and sealed	21
	Effect of δ_f on CL_α	Sealed	22(a)
	Effect of α on CL_δ	Sealed	22(b)
Pitching moment	$C_{m_\alpha}, C_{m_\delta}$, a.c., c.p. due to δ_f against M ($\alpha \approx 0^\circ, \delta_f = 0^\circ$)	Open and sealed	23
	Effect of δ_f on C_{m_α}	Sealed	24(a)
	Effect of α on C_{m_δ}	Sealed	24(b)
	Effect of δ_f on a.c.	Sealed	25
	Effect of α on c.p. due to δ_f	Sealed	25
Hinge moment	Ch_α against M ($\alpha \approx 0^\circ, \delta_f = 0^\circ$)	Open and sealed	26
	Effect of δ_f on Ch_α	Sealed	27
	Ch_δ against M ($\alpha \approx 0^\circ, \delta_f = 0^\circ$)	Open and sealed	28
	Effect of α on Ch_δ	Sealed	29
	Ch against δ_{TT} ($\alpha \approx 0^\circ, \delta_f = 0^\circ$)	Sealed	30

DISCUSSION OF RESULTS

BASIC DATA

Lift Characteristics

Lift due to angle of attack (figs. 8 and 9).- Compressibility had no adverse effect on the ability of the airfoil to develop lift in the low and moderate angle-of-attack ranges. At angles of attack near 10° , however, a sharp break occurred in the lift curves in the region $M = 0.95$. This break disappeared at $M = 1.05$ and higher speeds. As may be seen, the test range ($\alpha = 18^\circ$) was insufficient to yield information on the variation of maximum lift coefficient with Mach number. However, such information may be found for the model with a plain flap in reference 1.

The effect on shape of the lift curves of changing the flap angle from 0° to 5° was practically negligible. One of the small systematic changes noted was a delay to larger angles of attack in the occurrence of the sharp break in the lift curve near $M = 0.95$.

Sealing the flap gap had a beneficial effect on the lift characteristics of the model at angles of attack below approximately 8° . Inasmuch as only 64 percent of the gap length was sealed in the tests (refer to fig. 4), further gains in lifting ability could be expected from sealing a greater length of the flap gap.

Lift due to flap deflection (figs. 10 and 11).- The bevelled-trailing-edge flap showed generally good flap effectiveness. There was a considerable loss in effectiveness at small flap angles at $M = 0.95$ (fig. 10(a)) in the unsealed condition, which was alleviated by sealing the gap. In addition to this effect, the seal gave a worth-while overall improvement in flap effectiveness over most of the speed range tested. When the angle of attack was increased from 0° to 5° , the flap effectiveness was reduced somewhat.

The foregoing results appear on the surface to be at variance with other recent tests of controls with large trailing-edge angles made in wind-tunnels (references 3 and 4). These tests showed violent losses or even reversals in flap effectiveness in the transonic speed range with controls having somewhat smaller trailing-edge angles than that tested herein. The difference in results is probably due to the difference in airfoil section. The wind-tunnel tests were made with airfoil sections that have large trailing-edge angles which extend forward over approximately the entire flap chord. In the subject tests the large trailing-edge angle extended forward a distance equal to only one-fourth of the flap chord. Hence, it is possible in the subject

tests that part of the expected loss in flap effectiveness due to the large trailing-edge angle on the last $\frac{1}{4}$ chord of the flap was replaced by a gain in effectiveness from the forward $\frac{3}{4}$ -chord portion of the flap acting as a blunt trailing-edge control of smaller chord. If this analysis is borne out by further work, the conclusions to be drawn are that trailing-flap effectiveness at transonic speeds will be best for airfoil sections having their maximum thickness well forward in order to obtain a small over-all flap trailing-edge angle, and that flap effectiveness for a given airfoil section cannot be changed appreciably by local modifications to the contour of the flap short of resorting to a finite trailing-edge thickness (reference 5).

Pitching-Moment Characteristics

Pitching moment due to angle of attack (figs. 12 and 13).— These data showed no unusual variations. The seal did not change the pitching-moment characteristics appreciably except at high angles of attack where the pitching moments were increased by the addition of the seal.

Pitching moment due to flap deflection (figs. 14 and 15).— In general, the pitching moments due to flap deflection followed the same trends as the lift due to flap deflection. As in the case of the lift, the pitching moments also were increased considerably by sealing the flap gap. In figure 14 the data for the gap-open condition are apparently in error somewhat due to a zero shift.

Hinge-Moment Characteristics

Hinge moment due to angle of attack (figs. 16 and 17).— The hinge-moment-coefficient variations with angle of attack were very erratic with frequent changes between positive and negative floating tendencies below $\alpha \approx 8^\circ$ and below a Mach number of 1.0. Above $\alpha \approx 8^\circ$ the flap always exhibited a strong negative floating tendency. At supersonic speeds the curves tended to become linear and the flap had a strong negative floating tendency at all angles of attack.

A comparison between the (a) and (b) parts of the figures shows that the bevelled-trailing-edge flap was very susceptible to Reynolds number effects. Large Reynolds numbers gave greater positive floating tendencies in the low angle-of-attack range ($\alpha < 8^\circ$). The dependence of the bevelled-trailing-edge-flap hinge moments on Reynolds number is not surprising inasmuch as the balancing effectiveness of such controls depends on separation effects at the trailing edge which are, of course, influenced by Reynolds number.

The general shapes of the hinge-moment curves were not greatly affected by changing the flap angle from 0° to 5° .

Sealing the gap did not appreciably change the hinge-moment characteristics although it did tend to reduce the small-amplitude waviness in the hinge-moment curves near zero angle of attack.

The data indicate the hinge moment was not zero at zero flap deflection and zero angle of attack. The reason for this is believed to be small construction errors which introduced slight asymmetry into the model.

Hinge moment due to flap deflection (figs. 18 and 19).- As might be expected, the variation of hinge-moment coefficient with flap deflection at subsonic speeds was nonlinear. At Mach numbers of 1.0 and higher the curves became much steeper, indicating an abrupt loss in balance. Just as in the case of angle of attack, higher Reynolds numbers gave an increase in flap balance for deflection (compare figs. 18(a) and 18(b)).

Throughout the deflection range tested, the flap was generally less balanced with the gap sealed; however, the balance at small deflections was maintained to higher Mach numbers with the gap sealed. The data indicate the hinge moments with gap open were very irregular at low speeds near zero deflection. These irregularities were eliminated completely by sealing the gap.

Hinge moment due to tab deflection (fig. 20).- The trim-tab effectiveness is indicated by the vertical spacing of the curves of figure 20. At Mach numbers below 0.90, the tab gave increasing hinge moments of the correct sign with increasing tab deflection at zero flap deflection. At large positive flap angles the tab effectiveness reversed at small tab angles; whereas, at large negative flap angles the tab effectiveness usually reversed at larger tab angles. At Mach numbers above 0.90 the tab effectiveness usually reversed at moderate tab angles for all except large positive flap angles. Within the accuracy of the data, therefore, it appears the tab tested would constitute a weak if not entirely unsatisfactory trimming device.

SUMMARY DATA

Lift Characteristics

Lift-curve slope (figs. 21 and 22(a)).- The lift-curve slopes showed a general increase with increasing speed up to a Mach number of at least 1.0. At higher speeds the lift-curve slope fell off slightly.

Sealing the flap gap was definitely beneficial to increasing the lift-curve slope at all transonic speeds tested. The maximum lift-curve slope measured with gap sealed was 9 percent higher than the corresponding maximum lift-curve slope with gap open (fig. 21(a)). Reynolds number effects on lift-curve slope were small.

The effect of flap deflection on lift-curve slope was small and inconsistent (fig. 22(a)). At transonic speeds, deflecting the flap 5° reduced the lift-curve slope slightly.

Flap effectiveness (figs. 21 and 22(b)). - The absolute flap effectiveness (CL_δ) showed a gradual decrease over the speed range tested with an additional abrupt loss and recovery in effectiveness between $M = 0.90$ and $M = 1.05$. Sealing the gap gave a general increase in flap effectiveness over the speed range of about 25 percent. Other effects of the seal were to raise the Mach number of minimum flap effectiveness from 0.95 to 1.0 and to raise the minimum flap effectiveness by about 35 percent (fig. 21(a)). The data obtained from the level-flight runs (fig. 21(b)) were not as clear-cut as the high-dive data, but disregarding the apparent inconsistencies in the gap-sealed data, these data are in fair agreement with those of figure 21(a). The effectiveness of the bevelled flap compared favorably with that of the plain flap and horn-balanced flaps of references 1 and 2, respectively.

The variations of flap relative effectiveness $\frac{\partial \alpha}{\partial \delta_f}$ with Mach number were similar to those of absolute flap effectiveness (CL_δ).

The effect of increasing the angle of attack on flap effectiveness (fig. 22(b)) was to iron out variations in effectiveness due to compressibility. This result is in agreement with previous tests (reference 2).

Pitching-Moment Characteristics

Pitching-moment coefficient per degree angle of attack (figs. 23 and 24(a)). - The pitching-moment-coefficient slopes (C_{m_α}) were about constant below $M = 0.85$ and then increased considerably up to $M = 1.0$ after which they again tended to assume a constant value. Sealing the flap gap had little effect on the pitching-moment variations with angle of attack up to a Mach number of 0.95. Reynolds number effects and flap-deflection effects also did not change the pitching-moment variations at transonic speeds although some changes were indicated at subsonic speeds.

Pitching-moment coefficient per degree flap deflection (figs. 23 and 24(b)). - The variations of $C_{m\delta}$ with Mach number were very similar to those of $C_{L\delta}$ with Mach number. There was a greater increase in $C_{m\delta}$ due to sealing the gap than there was in $C_{L\delta}$. Also, as in the case of lift, the pitching-moment-slope variation due to compressibility was reduced greatly by changing the angle of attack from 0° to 5° . (See fig. 24(b).)

Aerodynamic-center location (figs. 23 and 25). - The aerodynamic-center position at low speeds varied between 10 and 20 percent mean aerodynamic chord depending on gap condition and Reynolds number. The Weissenger theory predicts an aerodynamic-center location of 20 percent mean aerodynamic chord for the plan form tested. In this connection it is known that thickening and bevelling the trailing edge tends to move the aerodynamic center forward. Also there is evidence that important lifting-surface effects come into play at low aspect ratios which are inadequately treated by the theory and cause a further forward shift in aerodynamic-center position.

In the subsonic speed range the effect of sealing the flap gap was to shift the aerodynamic center forward about 3 percent mean aerodynamic chord. Increasing the Reynolds numbers from those obtained in the high-dive runs to those obtained in the level-flight runs (fig. 6) caused an additional forward shift in aerodynamic center of about 5 percent mean aerodynamic chord.

Over the transonic speed range (up to $M = 1.15$) the aerodynamic center shifted rearward between 15 and 20 percent mean aerodynamic chord depending on Reynolds number and gap condition. All the data indicated an aerodynamic-center location of 25 percent mean aerodynamic chord at $M = 1.0$.

The effect on aerodynamic-center position of deflecting the flap 5° (fig. 25) was inconsistent at subsonic speeds. At transonic speeds, deflecting the flap 5° caused about a 2-percent rearward shift in aerodynamic-center position.

Center of pressure due to flap deflection (figs. 23 and 25). - The center of pressure due to flap deflection showed a rearward trend with increasing Mach number as in previous tests with other flaps (references 1 and 2). In spite of indicated random scatter of the data, the effect of sealing the flap gap is shown clearly. Closing the gap generally caused an appreciable rearward shift in center of pressure of the load caused by flap deflection. Such a rearward shift is beneficial to all-wing airplanes using ailerons as longitudinal control devices.

The effect of angle of attack on the center of pressure was generally small and inconsistent (fig. 25).

Hinge-Moment Characteristics

Flap floating tendency Ch_α (figs. 26 and 27).-- The bevelled flap showed large changes in floating tendency as measured by the instantaneous slopes of hinge-moment curves at $\alpha = 0^\circ$ over the test range. At subsonic speeds either increasing Mach number or increasing Reynolds number caused the flap to show greater positive (against the relative wind) floating tendencies. At about $M = 0.90$ this trend reversed so that at supersonic speeds the flap exhibited strong negative (with the relative wind) floating tendencies. Deflecting the flap 5° (fig. 27) reduced greatly the variation of Ch_α with either Mach number or Reynolds number in the subsonic speed range; however, at supersonic speeds the strong negative floating tendency still appeared. As explained in reference 2, it is believed the strong negative floating tendency at supersonic speeds is a feature common to all conventional types of subsonic balance which affect the parameter Ch_α . In any event the large changes in hinge-moment characteristics with angle of attack measured for the bevelled flap lead to the conclusion that this type of balance is undesirable for application to an airplane required to traverse any appreciable speed range.

Flap restoring tendency Ch_δ (figs. 28 and 29).-- Comparison of the bevelled-flap data (fig. 28) with that of the plain flap from reference 1 shows that the bevel was very effective as an aerodynamic balance in the subsonic range. However, in general, the degree of balance obtained from the bevelled trailing edge was far from uniform, ranging anywhere from one-half of complete unbalance to overbalance. As in the case of the variations of hinge moment with angle of attack, the degree of flap balance for deflection increased with either Mach number or Reynolds number in the subsonic speed range. At supersonic speeds the flap quickly lost balance as was the case with the horn-balanced flap of reference 2. Sealing the flap gap tended to delay the loss of balance at supersonic speeds, but the trends of the curves leave little hope that the bevelled trailing edge tested could be an effective supersonic balancing device.

Changing the angle of attack from 0° to 5° (fig. 29) had little effect on the subsonic balancing characteristics. The main effect was to hasten the loss of balance in the transonic speed range.

These small-scale data indicate the bevelled-trailing-edge flap as tested is an unsuitable form of aerodynamic balance for airplanes required to traverse a large speed range because of nonuniform balancing characteristics at subsonic speeds and inability to maintain aerodynamic balancing effectiveness through the transonic speed range.

Trim-tab effectiveness (fig. 30). - The bevelled trim tab gave hinge moments of the correct sign with increasing tab deflection at speeds below $M = 0.90$ for zero flap deflection and zero angle of attack. At $M = 0.90$, however, the data indicated complete tab ineffectiveness for the first 2° of tab deflection. At $M = 0.95$ the data showed complete tab ineffectiveness at deflections above 5° . At and above sonic speed the data indicated reversal in tab effectiveness above 3° to 5° of tab deflection.

CONCLUSIONS

On the basis of wing-flow tests of a full-span $\frac{1}{4}$ -chord flap having a 23° bevelled trailing edge mounted on a 35° sweptback untapered NACA 65-009 airfoil model of aspect ratio 3.07, the following conclusions were reached:

1. The lift characteristics of the model and flap were similar to those measured previously with true-contour flaps on the model.
2. Sealing the flap gap increased the lift-curve slope and the flap effectiveness appreciably and caused a rearward shift in the center of pressure of the load due to flap deflection.
3. The $\frac{1}{3}$ -flap-chord by $\frac{1}{3}$ -flap-span bevelled trim tab had unsatisfactory characteristics at all speeds tested inasmuch as the tab showed reversal of effectiveness over various parts of the deflection range at different Mach numbers.
4. The bevelled trailing edge appears to be an unsatisfactory type of aerodynamic balance for airplanes required to traverse a large speed range because at subsonic speeds the degree of balance was highly nonuniform (varying considerably with both Mach and Reynolds numbers) and at low supersonic speeds most of the balancing effectiveness disappeared.

Langley Aeronautical Laboratory
National Advisory Committee for Aeronautics
Langley Air Force Base, Va.

R E F E R E N C E S

1. Johnson, Harold I.: Measurements of Aerodynamic Characteristics of a 35° Sweptback NACA 65-009 Airfoil Model with $\frac{1}{4}$ -Chord Plain Flap by the NACA Wing-Flow Method. NACA RM L7F13, 1947.
2. Johnson, Harold I., and Brown, B. Porter: Measurements of Aerodynamic Characteristics of a 35° Sweptback NACA 65-009 Airfoil Model with $\frac{1}{4}$ -Chord Horn-Balanced Flap by the NACA Wing-Flow Method. NACA RM L9B23a, 1949.
3. Boddy, Lee E., and Morrill, Charles P., Jr.: The Aerodynamic Effects of Modifications to the Wing and Wing-Fuselage Intersection of an Airplane Model with the Wing Swept Back 35° . NACA RM A7J02, 1947.
4. Turner, Thomas R., Lockwood, Vernard E., and Vogler, Raymond D.: Preliminary Investigation of Various Ailerons on a 42° Sweptback Wing for Lateral Control at Transonic Speeds. NACA RM L8D21, 1948.
5. Turner, Thomas R., Lockwood, Vernard E., and Vogler, Raymond D.: Aerodynamic Characteristics at Subsonic and Transonic Speeds of a 42.7° Sweptback Wing Model Having an Aileron with Finite Trailing-Edge Thickness. NACA RM L8K02, 1949.

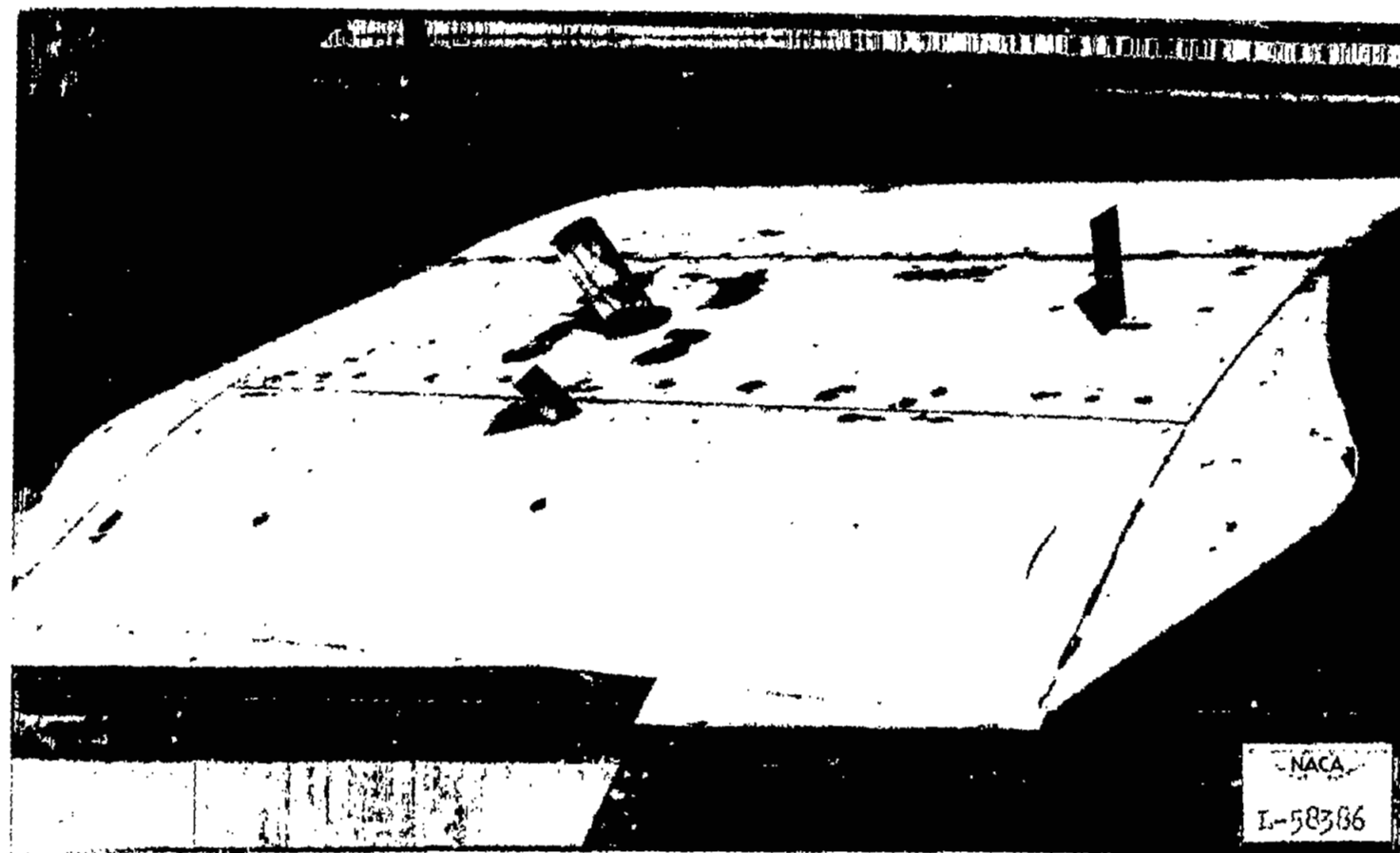


Figure 1.- View of 35° sweptback 65-009 model having $\frac{1}{4}$ -chord bevelled-trailing-edge flap mounted on right wing of F-51D airplane. Rectangular vane on right used for measuring angle of attack. Sweptback vane on left used for measuring downwash.

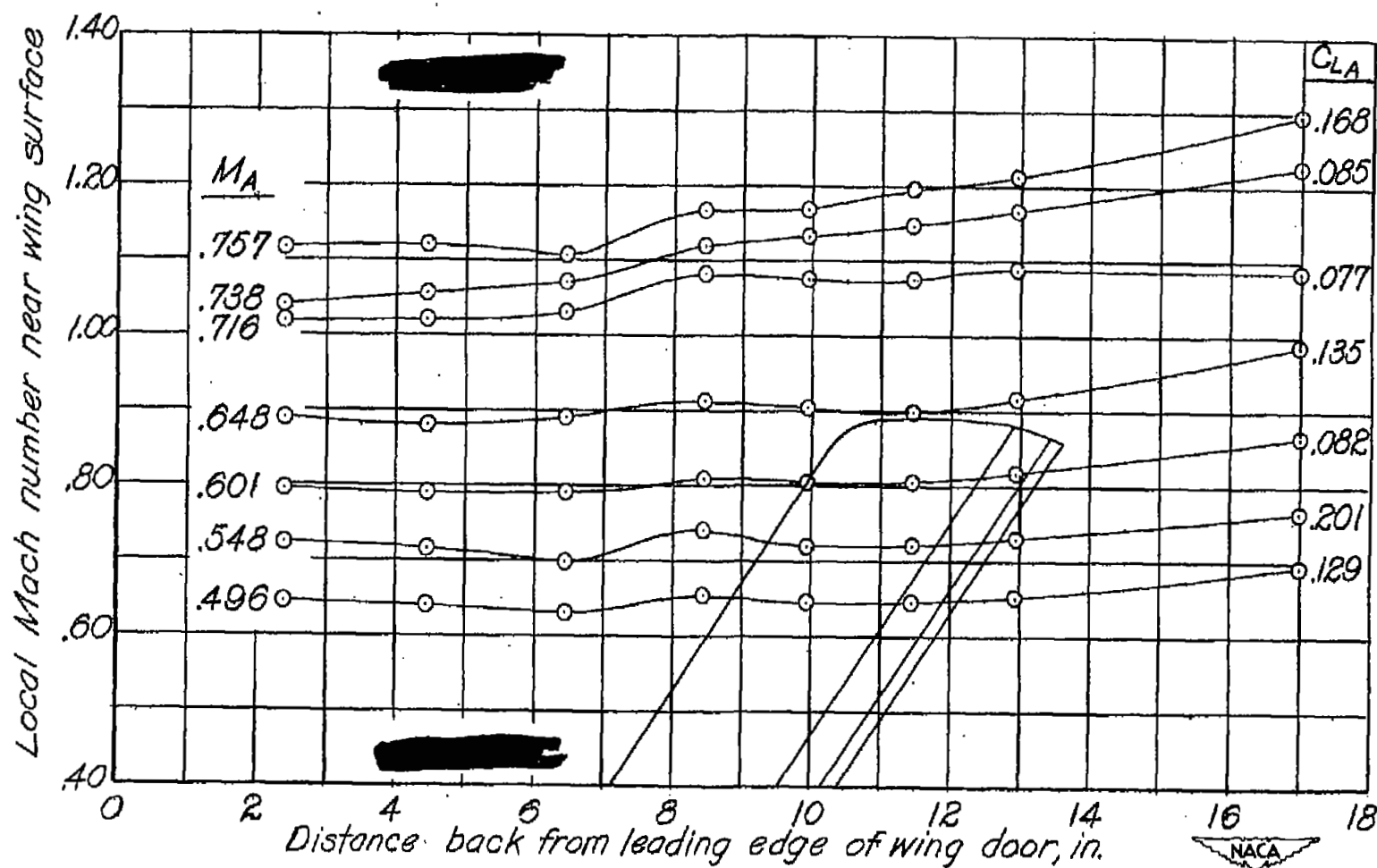


Figure 2.- Typical variations of local Mach number near wing surface with chordwise distance along wing surface for various airplane Mach numbers and lift coefficients as measured with model removed. Model location indicated by sketch.

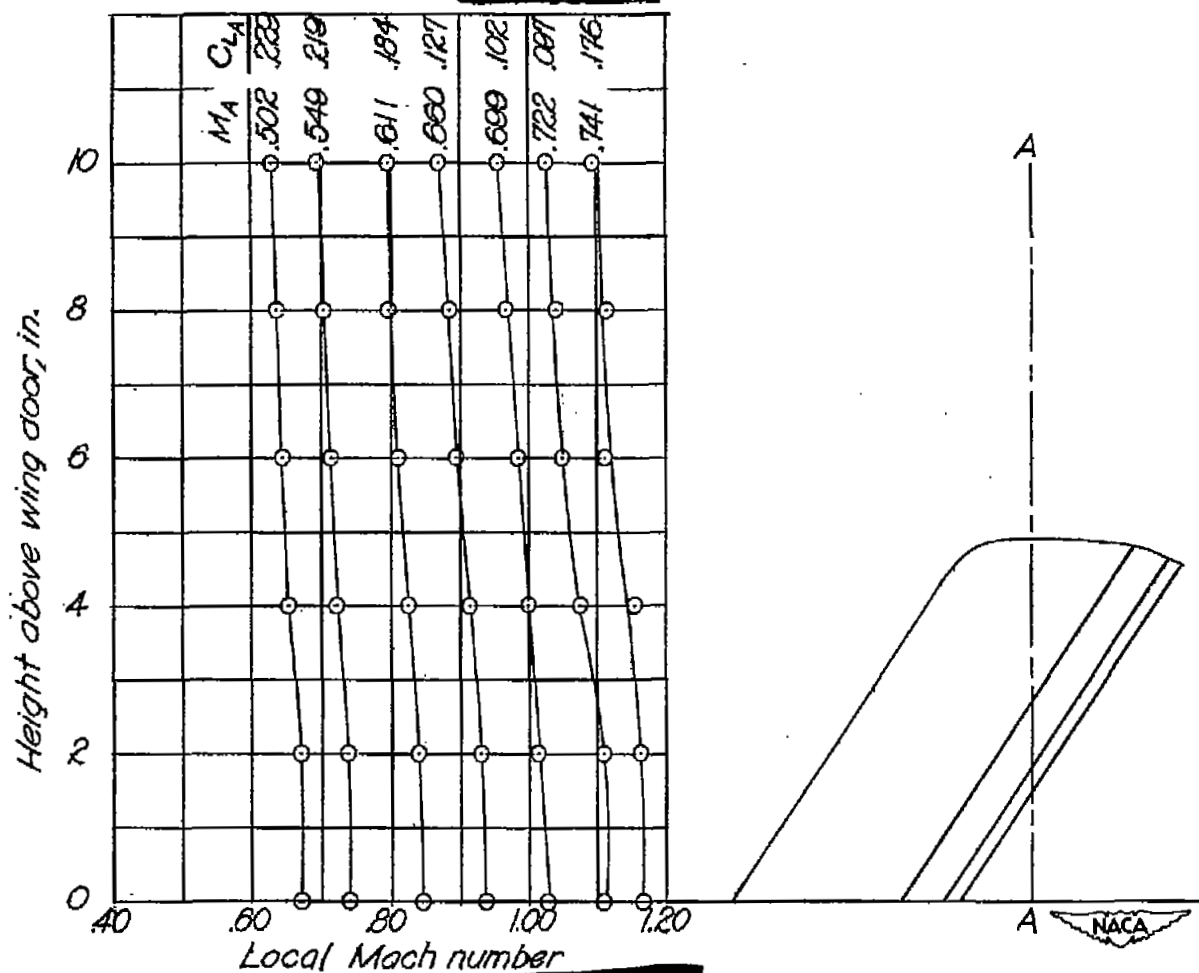


Figure 3.- Typical variations of local Mach number with vertical distance above wing surface as measured at chordwise station AA with model removed. Measurements made on left wing which had same contour as right wing. No allowance made for wing boundary layer.

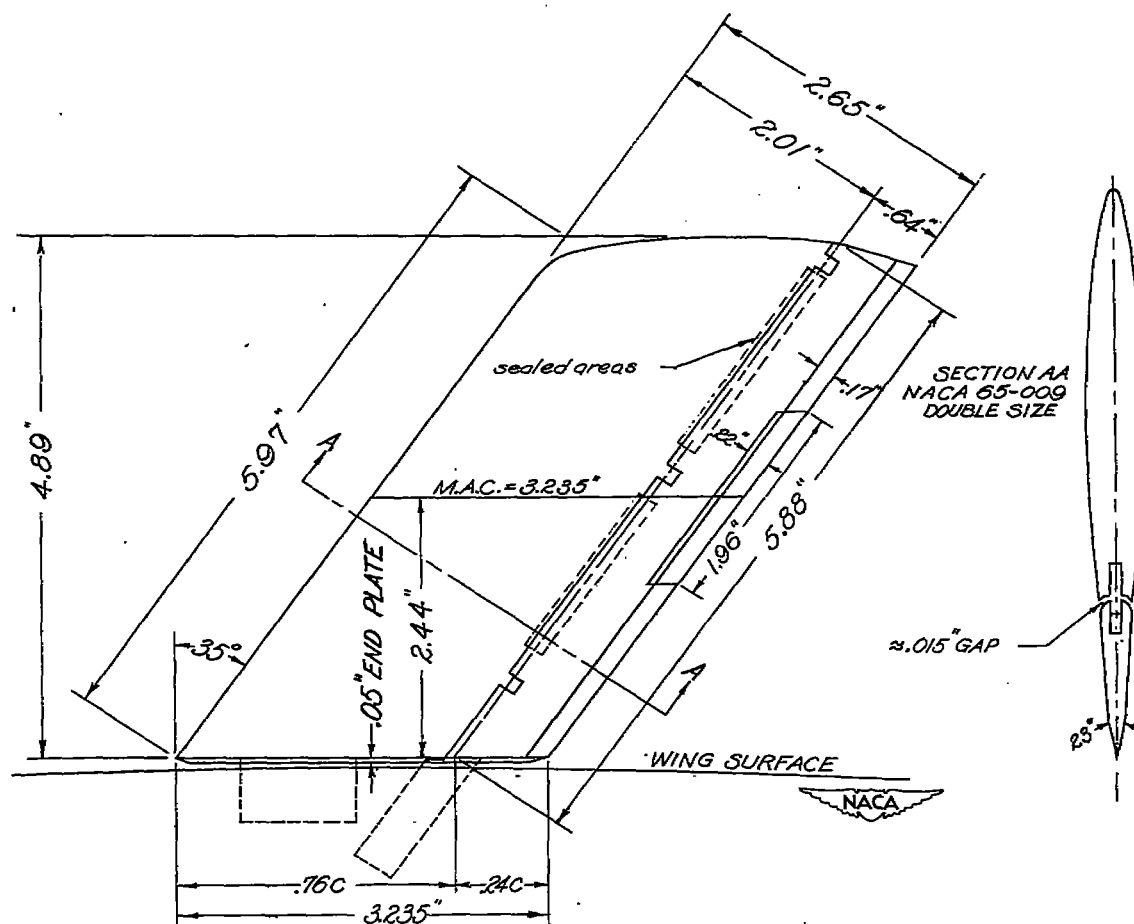
$$\begin{aligned} \mu &= 35^\circ \\ \lambda &= 1.0 \\ A &= 3.07 \\ b &= 4.89 \text{ in.} \\ \bar{c} &= 3.235 \text{ in.} \\ S &= 15.57 \text{ in.}^2 \end{aligned}$$
$$\begin{aligned} b_f &= 5.88 \text{ in.} \\ c_f &= .24 \text{ c} \\ \bar{c}_f &= .64 \text{ in.} \\ S_f &= 3.69 \\ \phi &= 23^\circ \end{aligned}$$
$$\begin{aligned} b_{TT} &= 1.96 \text{ in.} \\ \bar{c}_{TT} &= .22 \text{ in.} \\ \bar{c}_{TT}/\bar{c}_f &= .34 \\ S_{TT} &= .43 \text{ in.}^2 \\ S_{TT}/S_f &= .116 \end{aligned}$$


Figure 4.- Plan form and cross section of 35° sweptback NACA 65-009 airfoil with 24-percent-chord full-span, bevelled-trailing-edge flap.

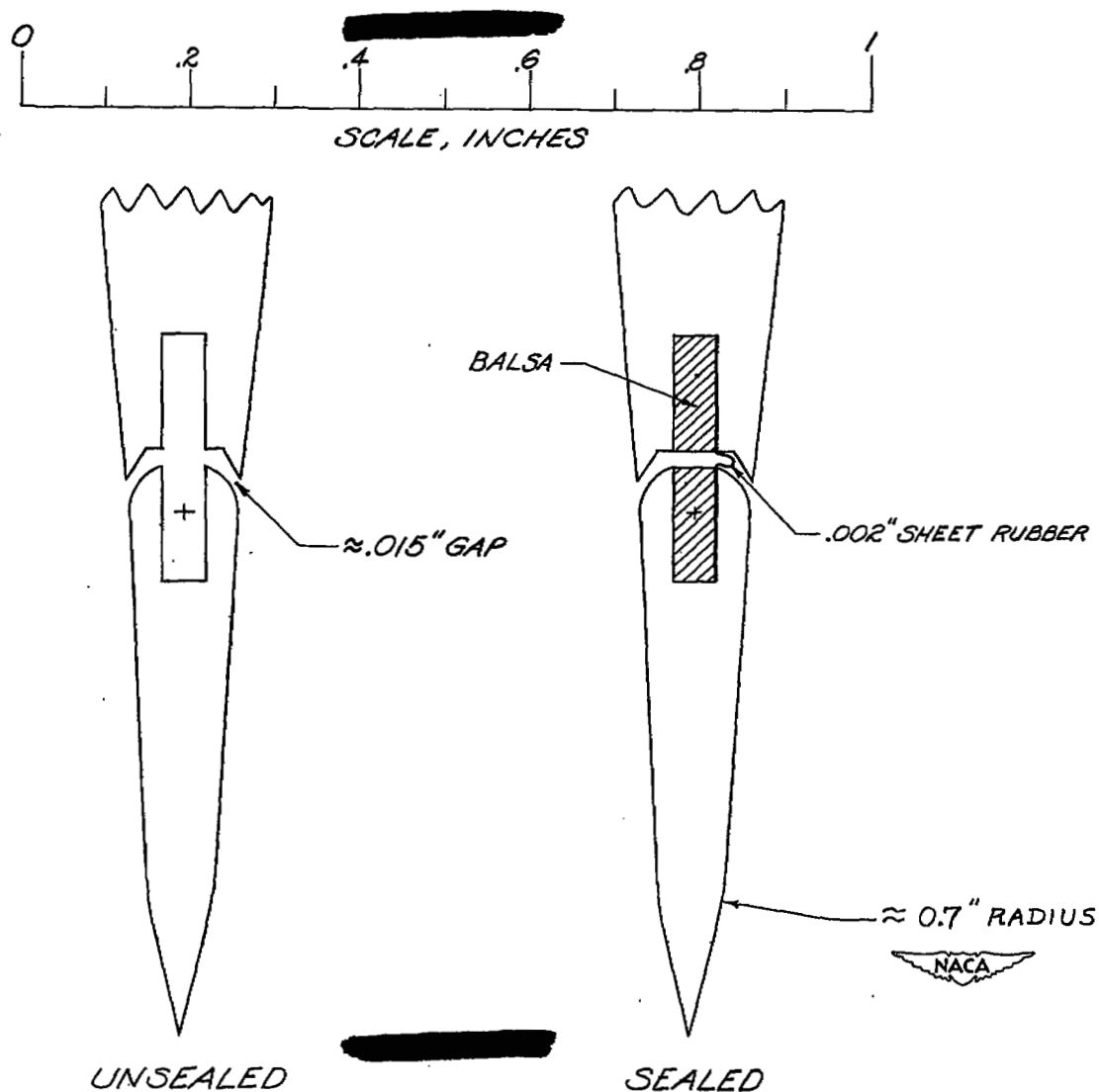


Figure 5.- Enlarged sectional views showing unsealed- and sealed-gap conditions.

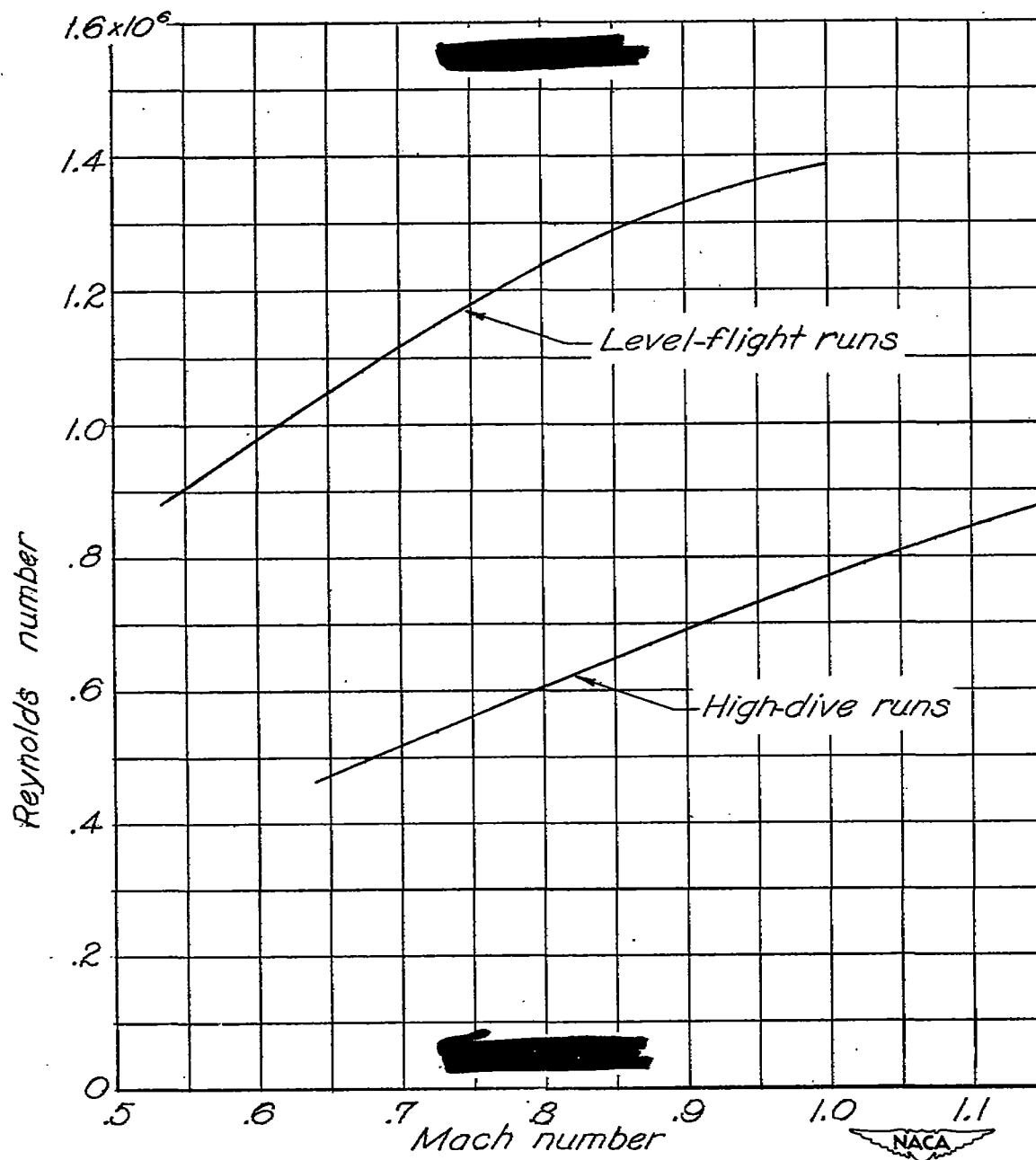
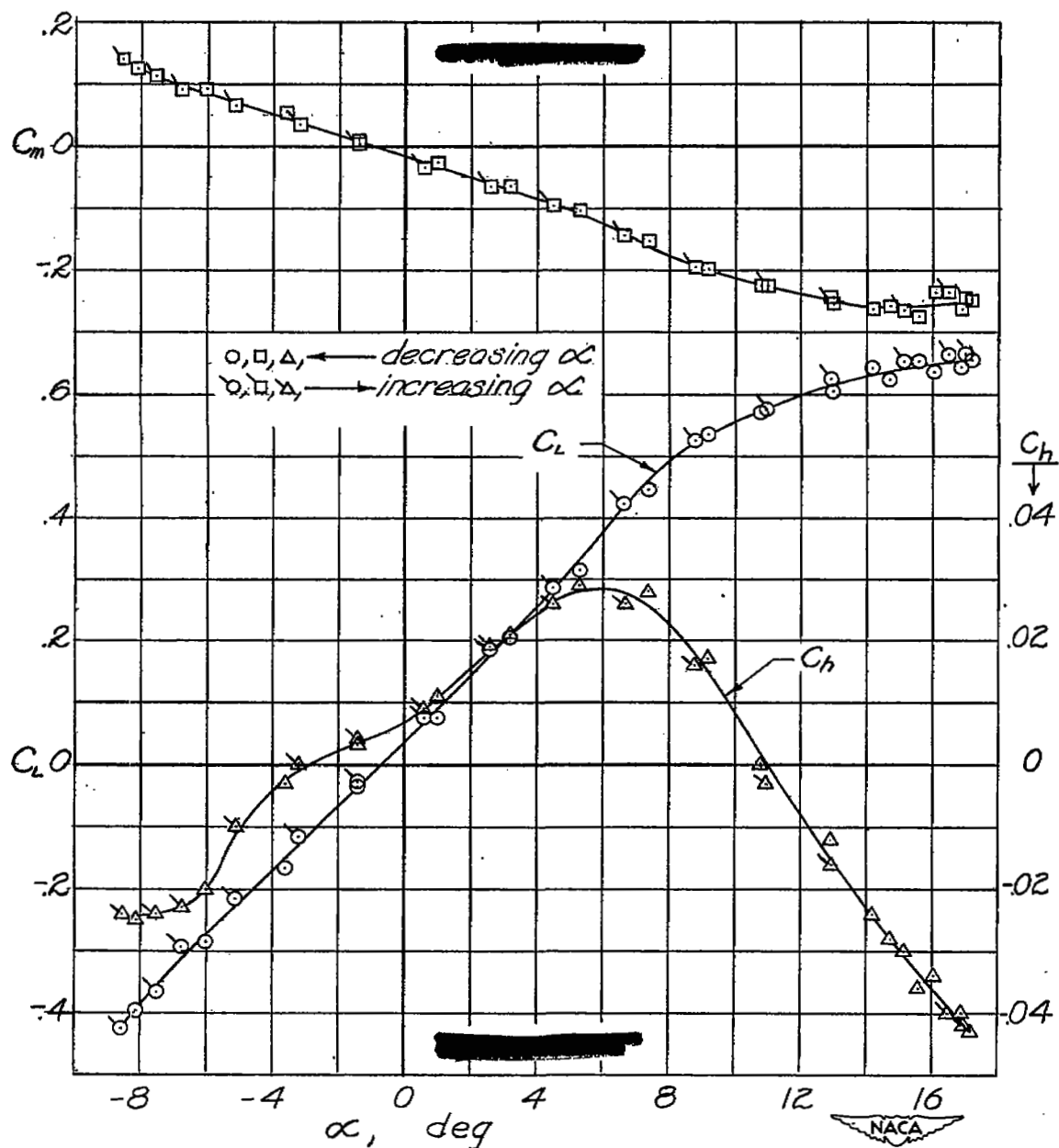
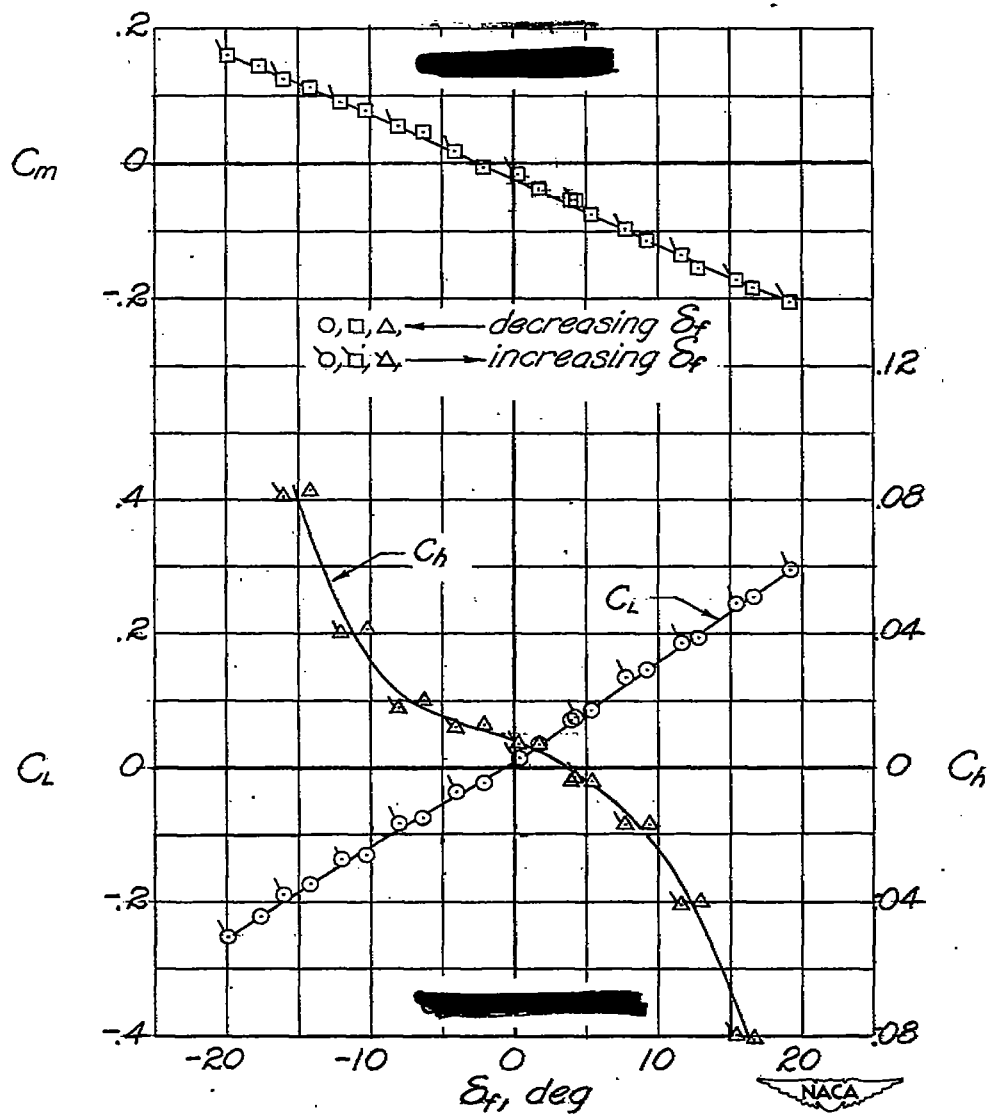


Figure 6.- Variation of Reynolds number with Mach number for tests of 35° sweptback, NACA 65-009 airfoil model with $\frac{1}{4}$ -chord bevelled-trailing-edge flap by the NACA wing-flow method. Reynolds number based on airfoil chord parallel to direction of flow.



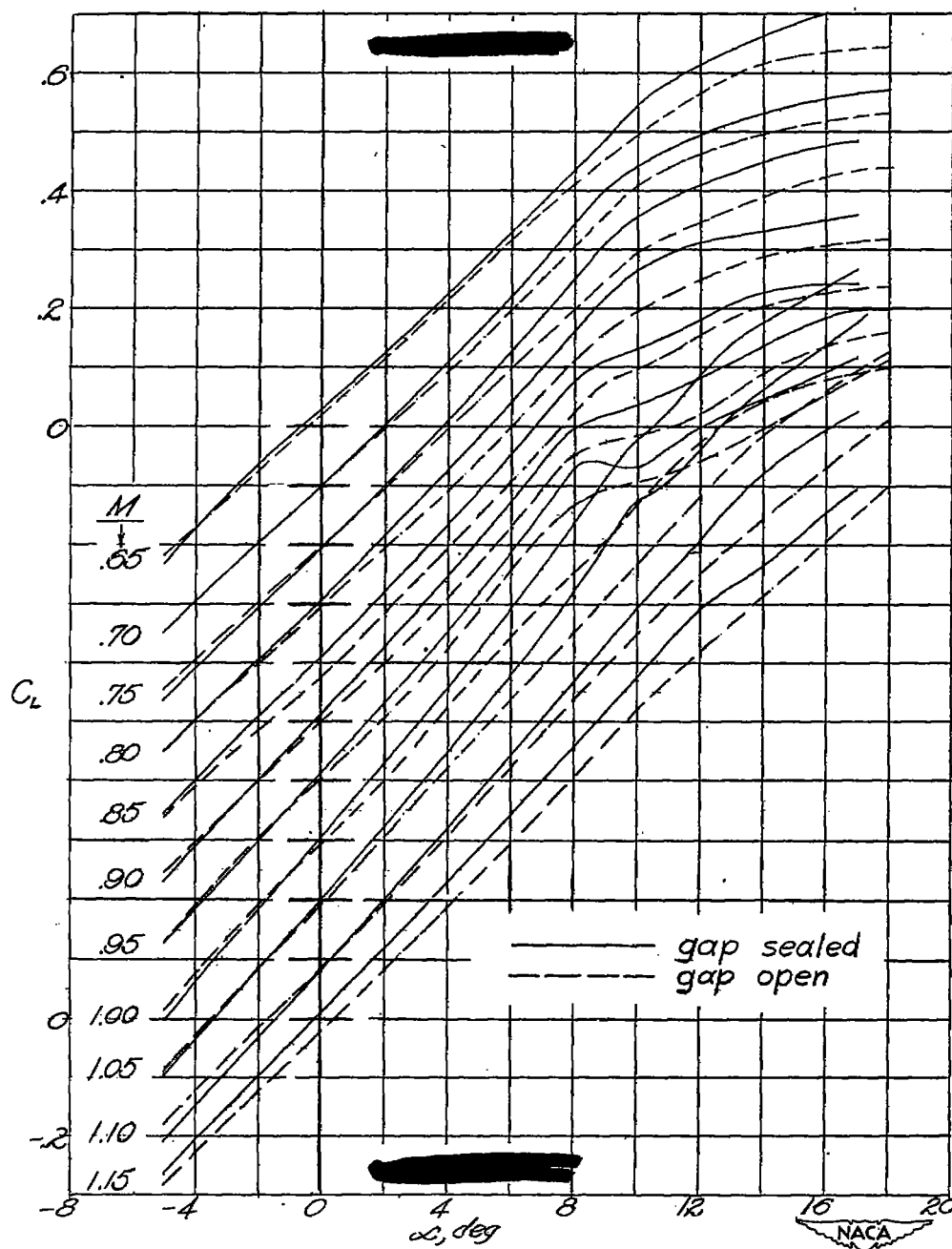
(a) Variation of C_L , C_m , and C_h with angle of attack.

Figure 7.- Typical examples of data obtained from strain-gage balance.
 NACA 65-009 airfoil, $A = 3.07$, $\Lambda = 35^\circ$, $c_f = 0.24c$, gap unsealed,
 bevelled-trailing-edge flap. Level-flight run, $M = 0.85$.



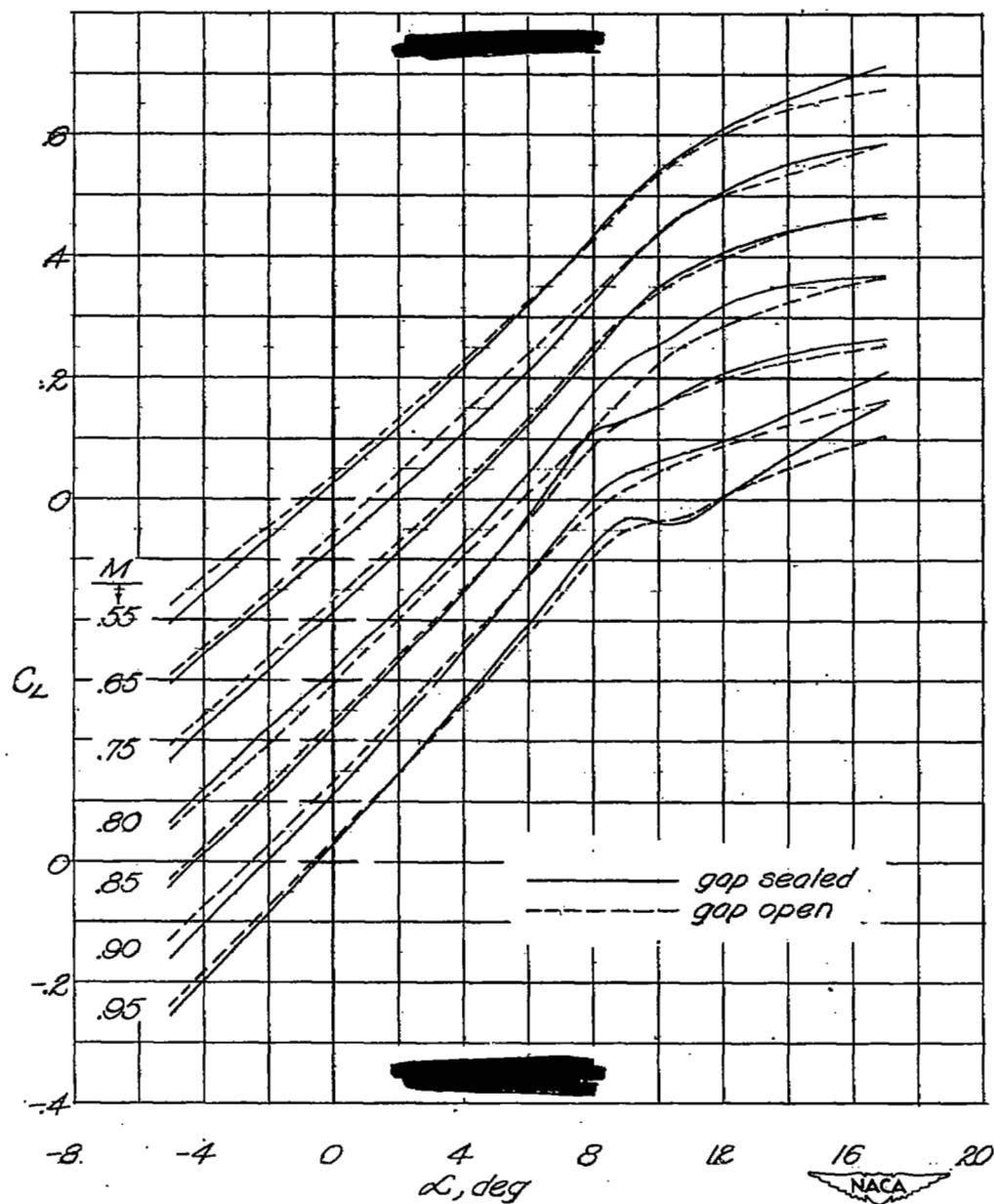
(b) Variation of C_L , C_m , and C_h with flap deflection.

Figure 7.- Concluded.



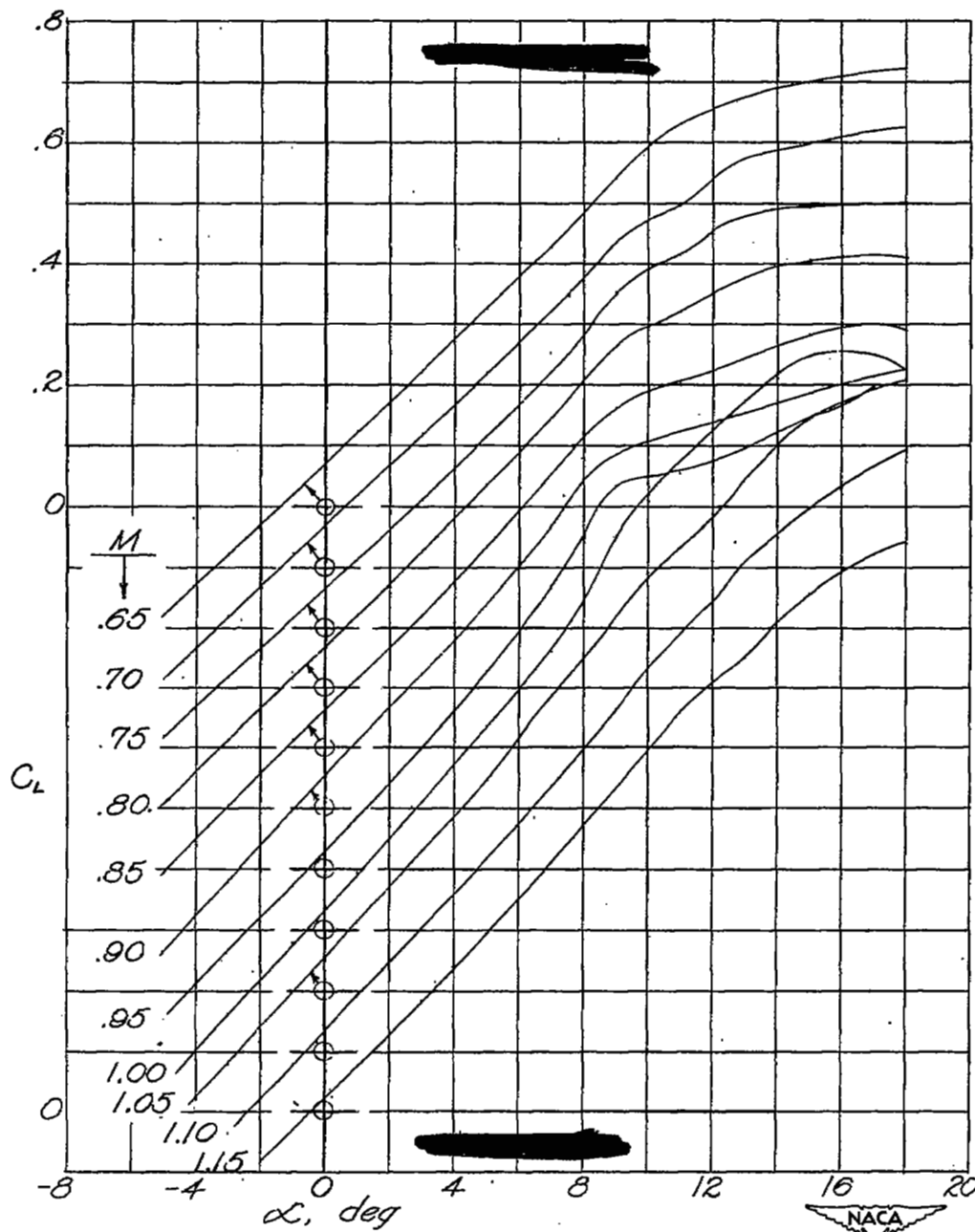
(a) High-dive runs.

Figure 8.- Variation of lift coefficient with angle of attack throughout Mach number range tested for $\delta_f = 0^\circ$. NACA 65-009 airfoil, $A = 3.07$, $\Lambda = 35^\circ$, $c_f = 0.24c$, gap sealed and unsealed, bevelled-trailing-edge flap. Note shift in axis of ordinate scale for different Mach numbers.



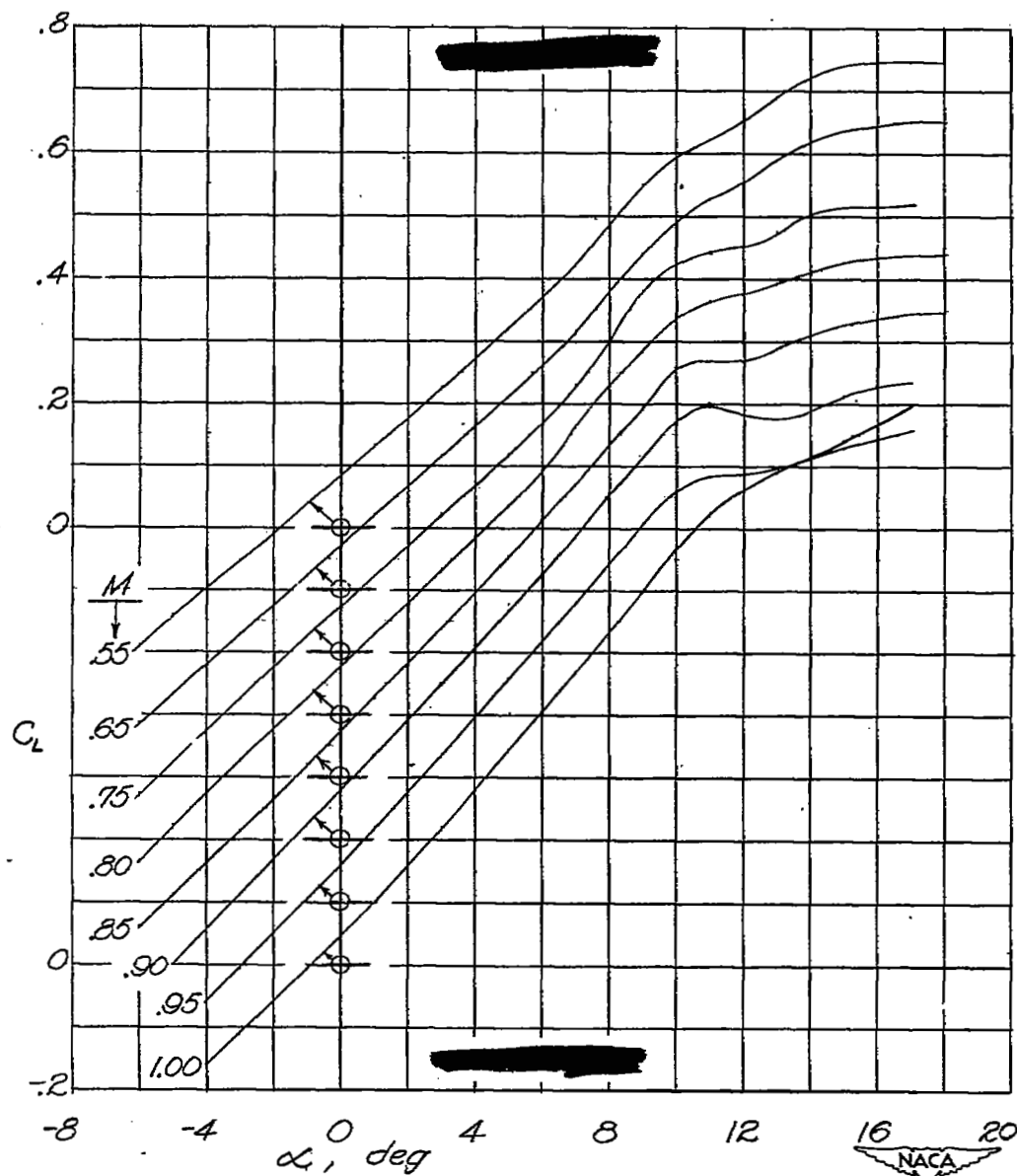
(b) Level-flight runs.

Figure 8.- Concluded.



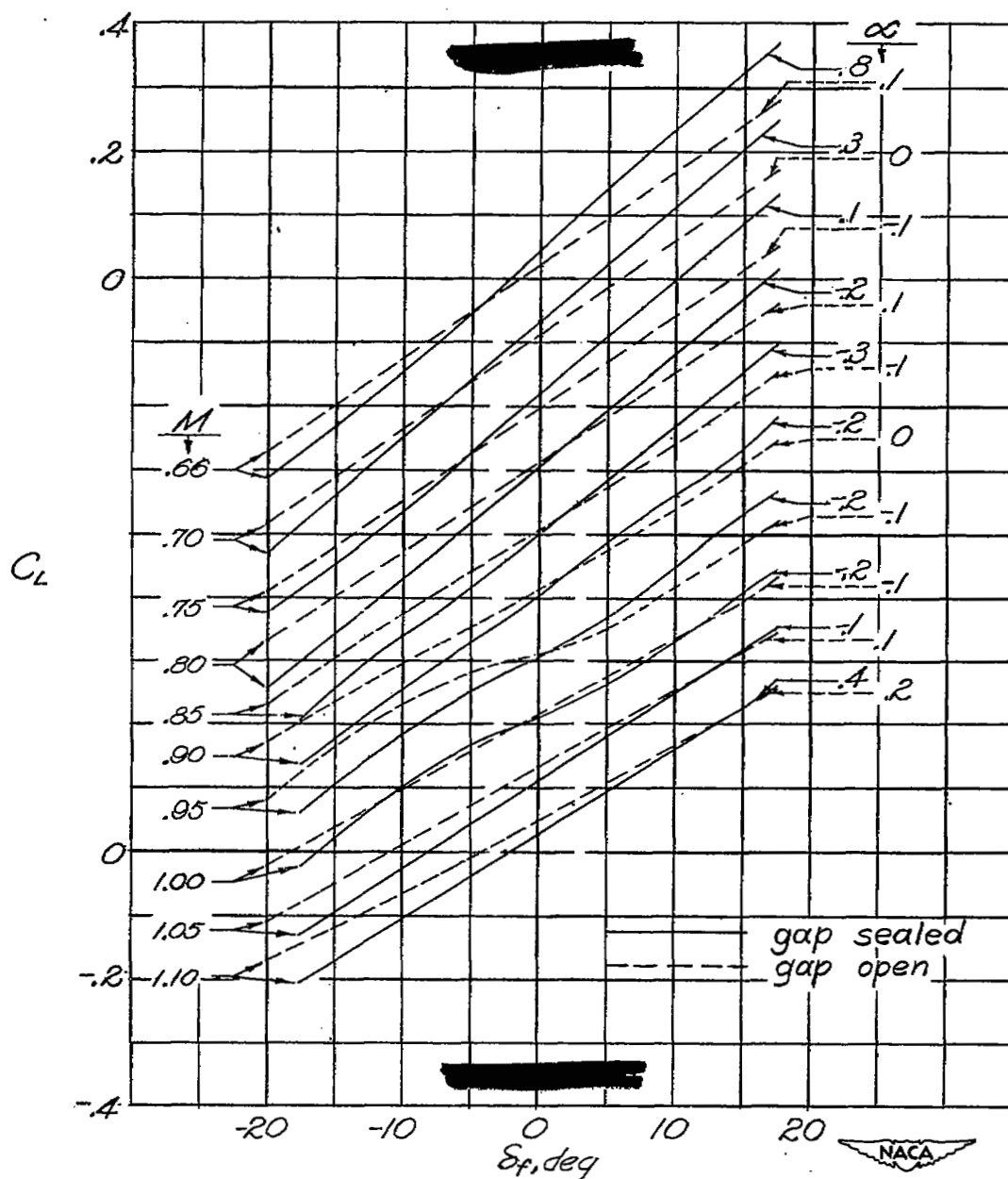
(a) High-dive runs.

Figure 9.- Variation of lift coefficient with angle of attack throughout Mach number range tested for $\delta_f = 5^\circ$. NACA 65-009 airfoil, $A = 3.07$, $\Lambda = 35^\circ$, $c_f = 0.24c$, gap sealed, bevelled-trailing-edge flap. Note shift in axis of ordinate scale for different Mach numbers.



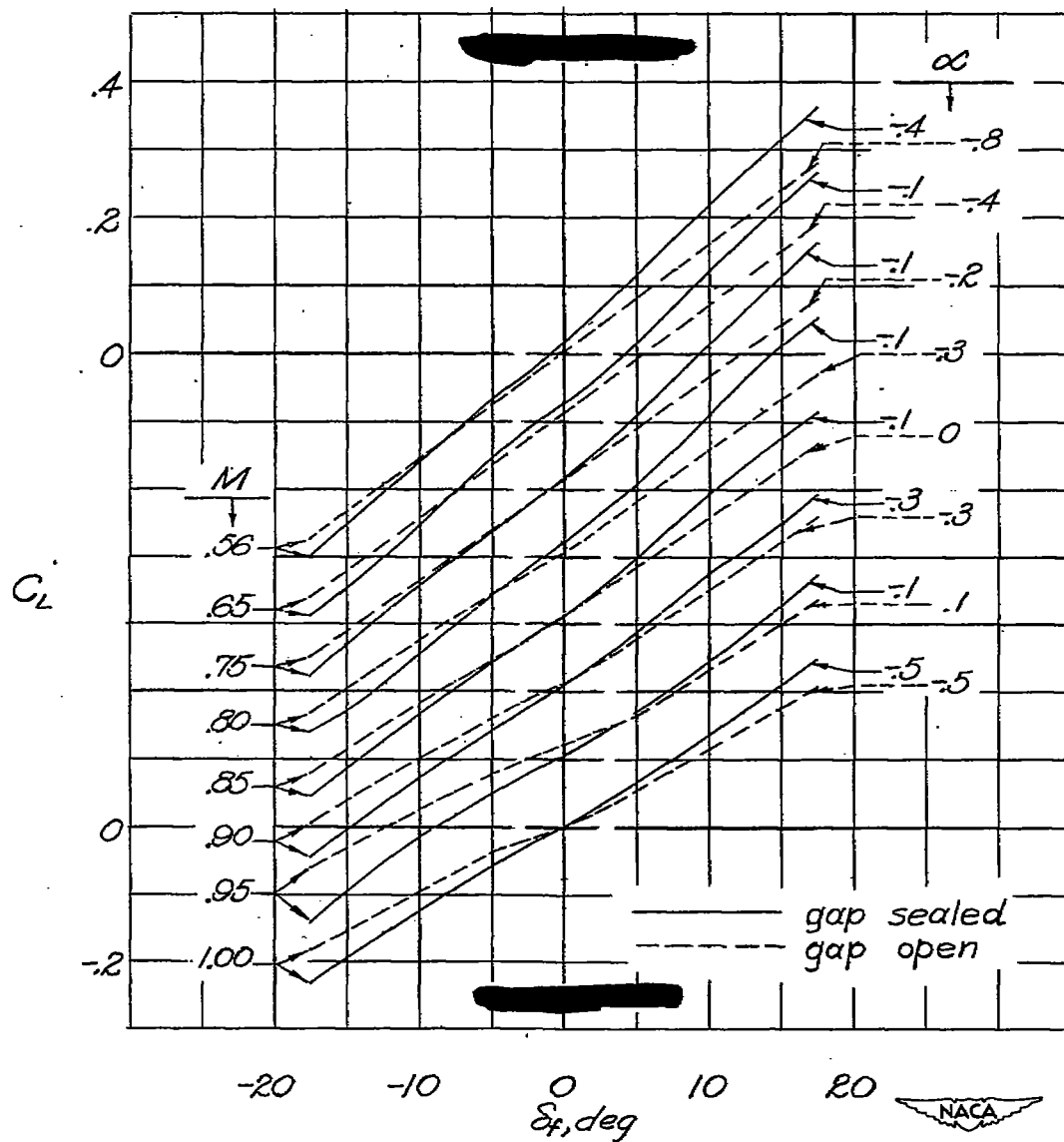
(b) Level-flight runs.

Figure 9.- Concluded.



(a) High-dive runs.

Figure 10.- Variation of lift coefficient with flap deflection throughout Mach number range tested for $\alpha \approx 0^\circ$. NACA 65-009 airfoil, $A = 3.07$, $\Lambda = 35^\circ$, $c_f = 0.24c$, gap sealed and unsealed, bevelled-trailing-edge flap. Note shift in axis of ordinate scale for different Mach numbers.



(b) Level-flight runs.

Figure 10.- Concluded.

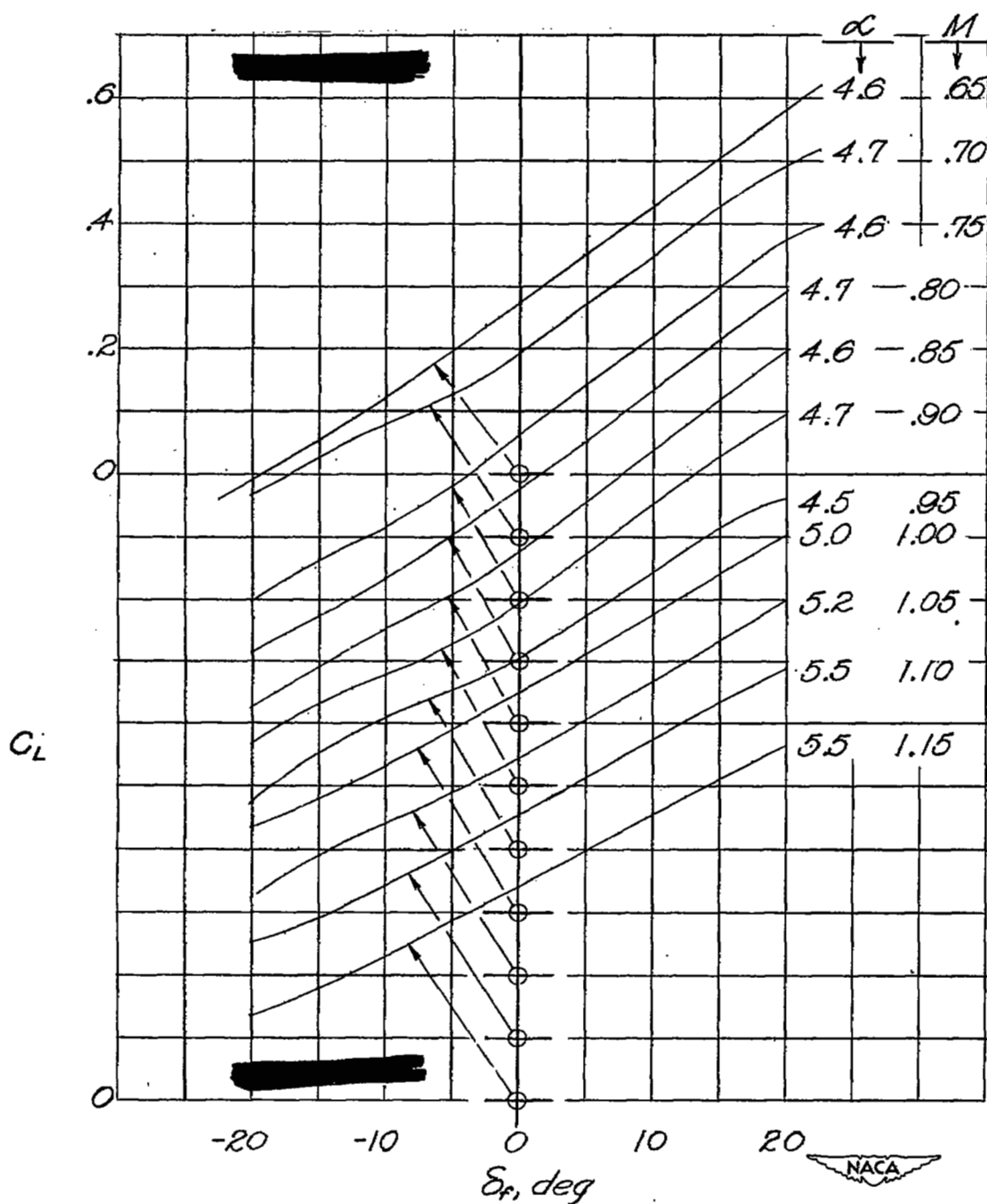
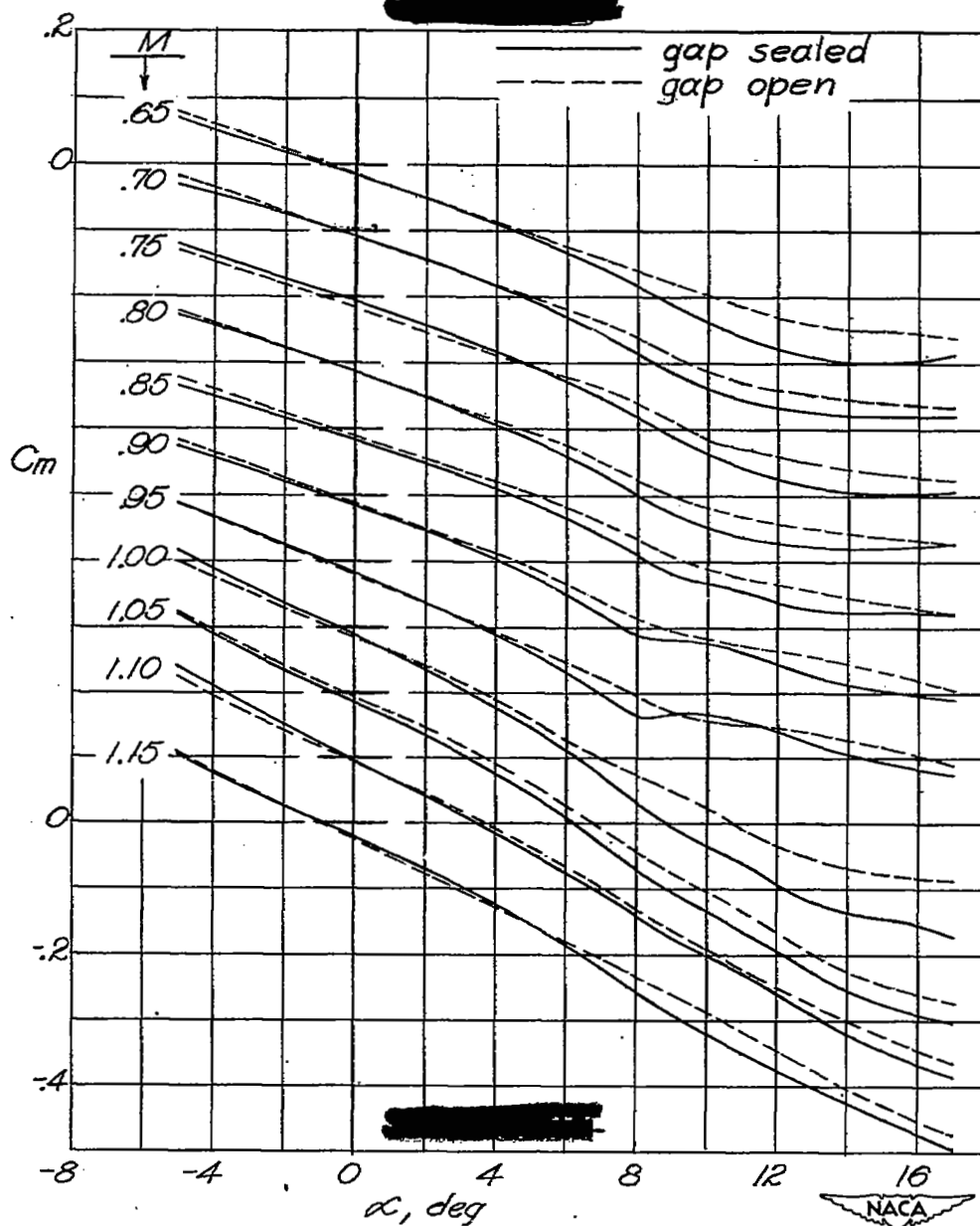
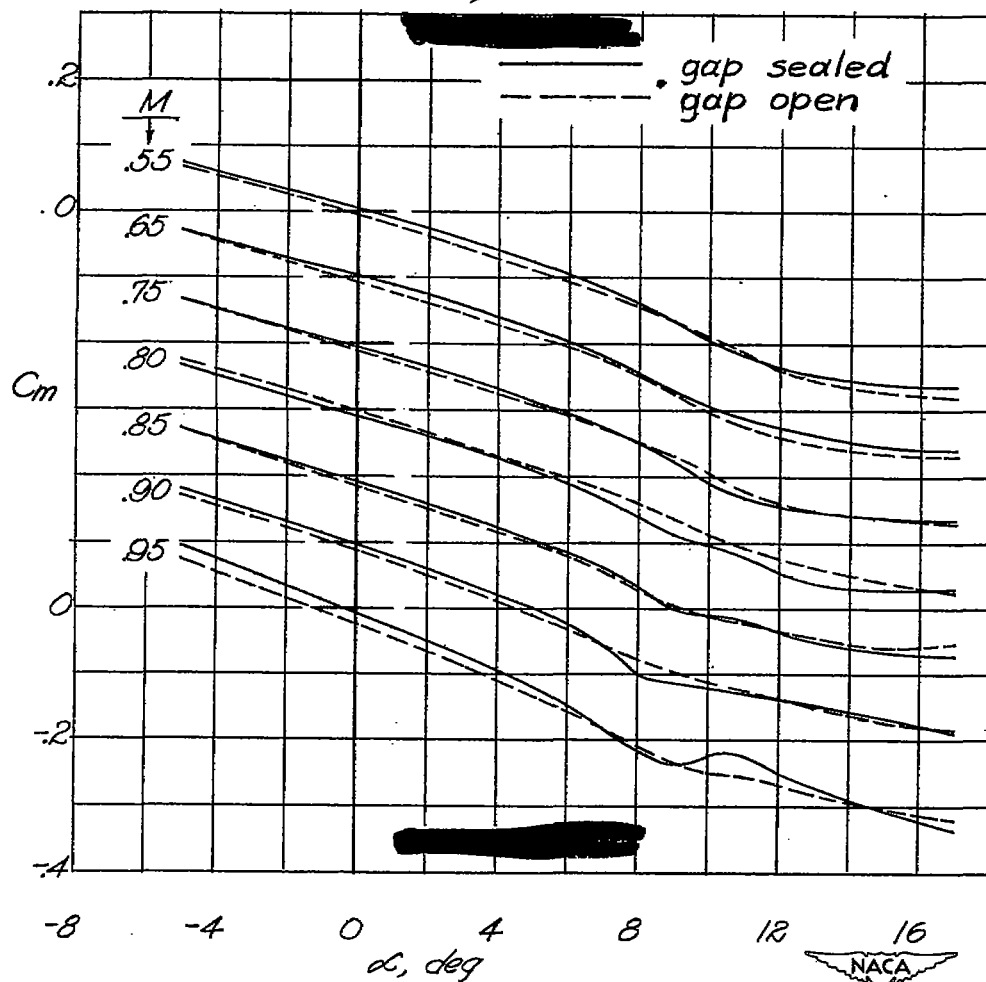


Figure 11.- Variation of lift coefficient with flap deflection throughout Mach number range tested for $\alpha \approx 5^\circ$. NACA 65-009 airfoil, $A = 3.07$, $\Lambda = 35^\circ$, $c_f = 0.24c$, gap sealed, bevelled-trailing-edge flap. Note shift in axis of ordinate scale for different Mach numbers. High-dive runs.



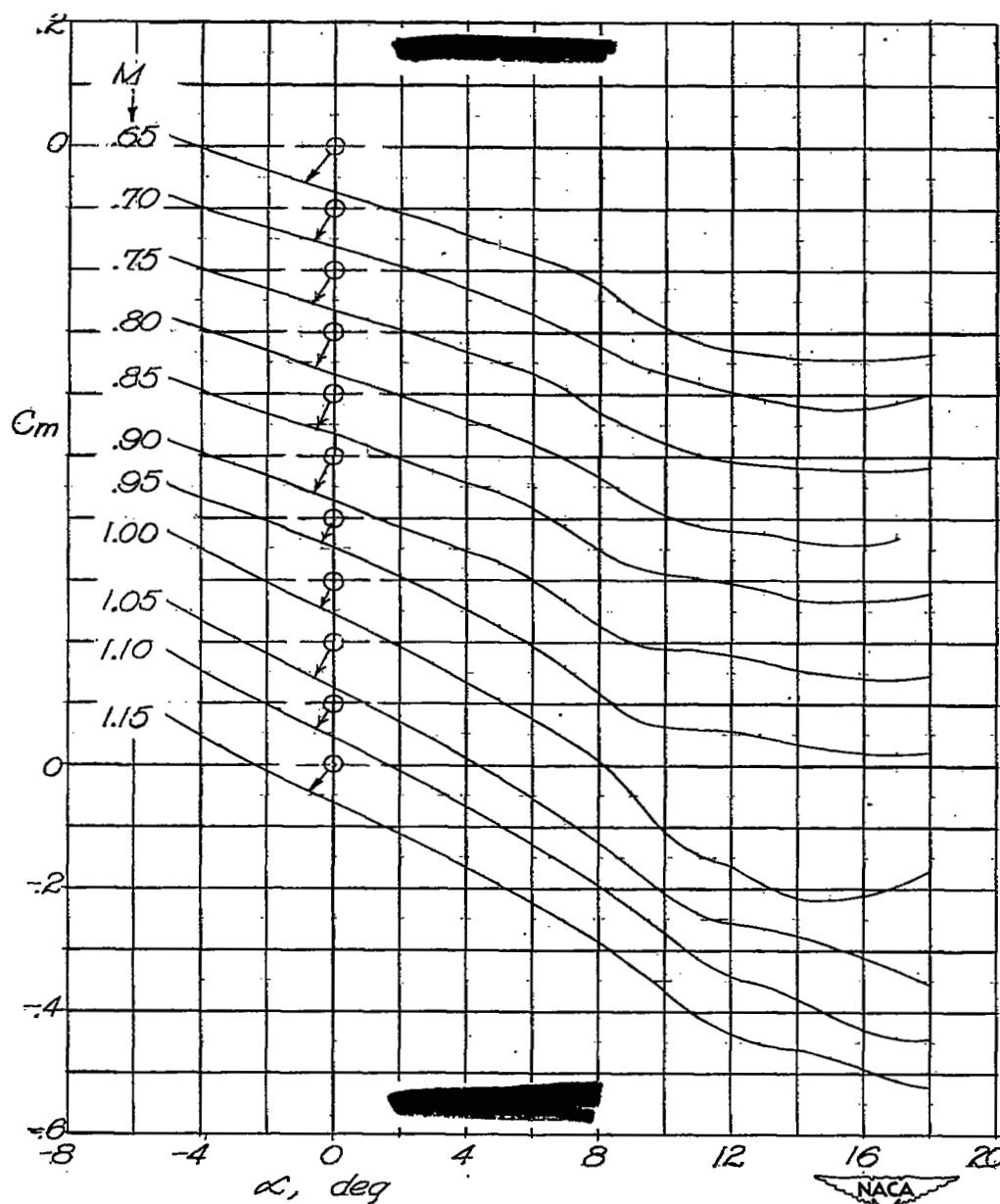
(a) High-dive runs.

Figure 12.- Variation of pitching-moment coefficient with angle of attack throughout Mach number range tested for $\delta_f = 0^\circ$. NACA 65-009 airfoil, $A = 3.07$, $\Lambda = 35^\circ$, $c_f = 0.24c$, gap sealed and unsealed, bevelled-trailing-edge flap. Moment coefficient given about axis located 18.1 percent mean aerodynamic chord ahead of leading edge of mean aerodynamic chord. Note shift in axis of ordinate scale for different Mach numbers.



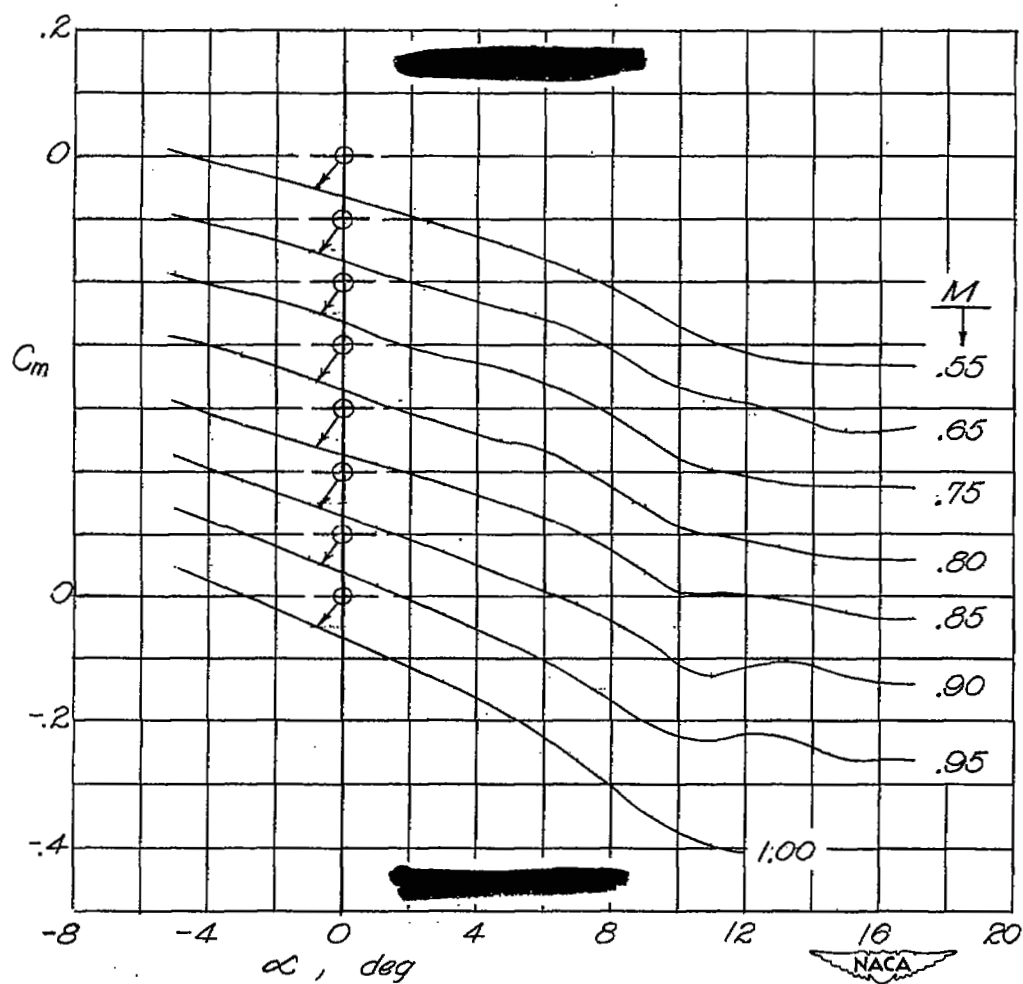
(b) Level-flight runs.

Figure 12.- Concluded.



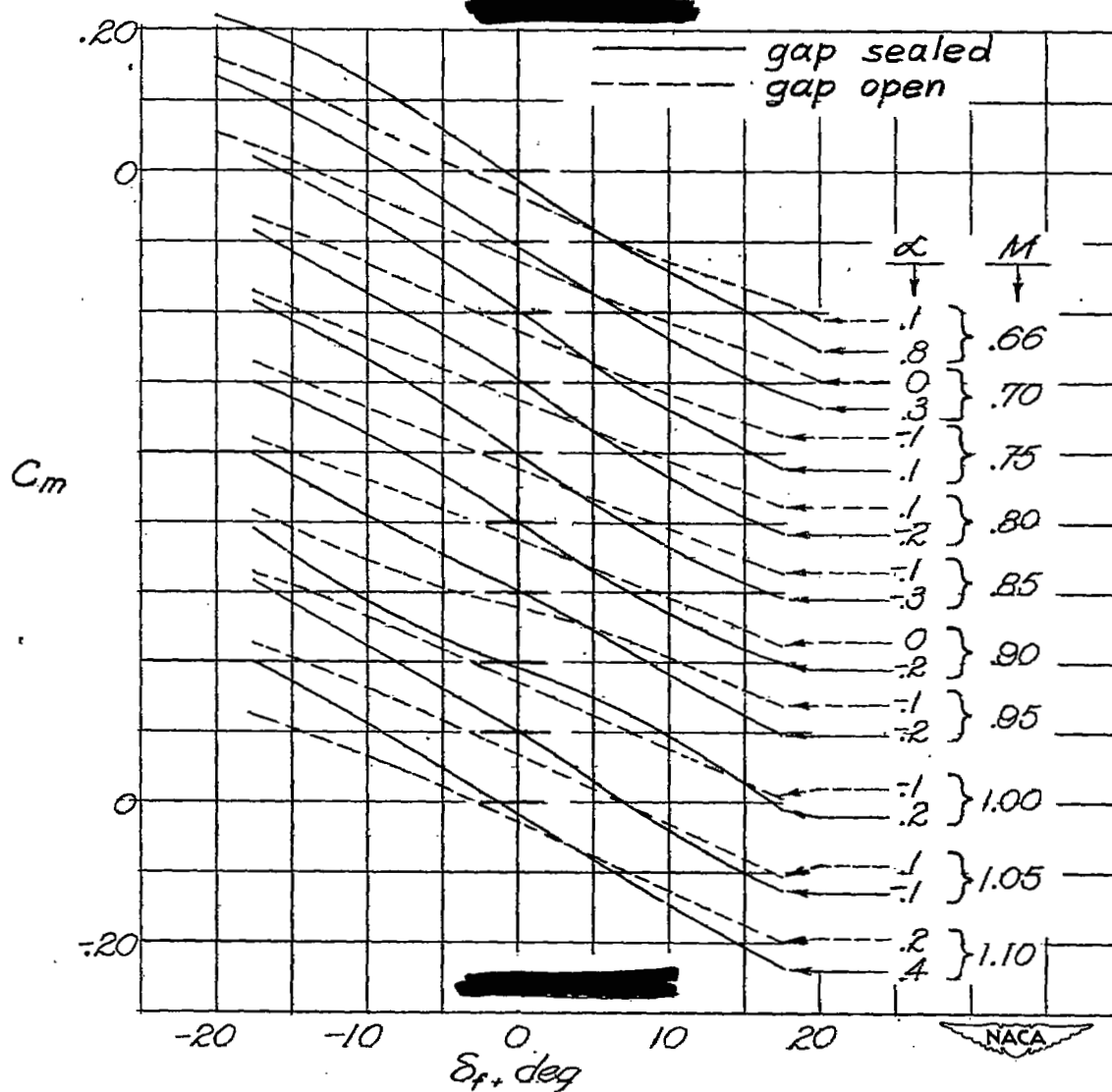
(a) High-dive runs.

Figure 13.- Variation of pitching-moment coefficient with angle of attack throughout Mach number range tested for $\delta_f = 5^\circ$. NACA 65-009 airfoil, $A = 3.07$, $\Lambda = 35^\circ$, $c_f = 0.24c$, gap sealed, bevelled-trailing-edge flap. Moment coefficient given about axis located 18.1 percent mean aerodynamic chord ahead of leading edge of mean aerodynamic chord. Note shift in axis of ordinate scale for different Mach number.



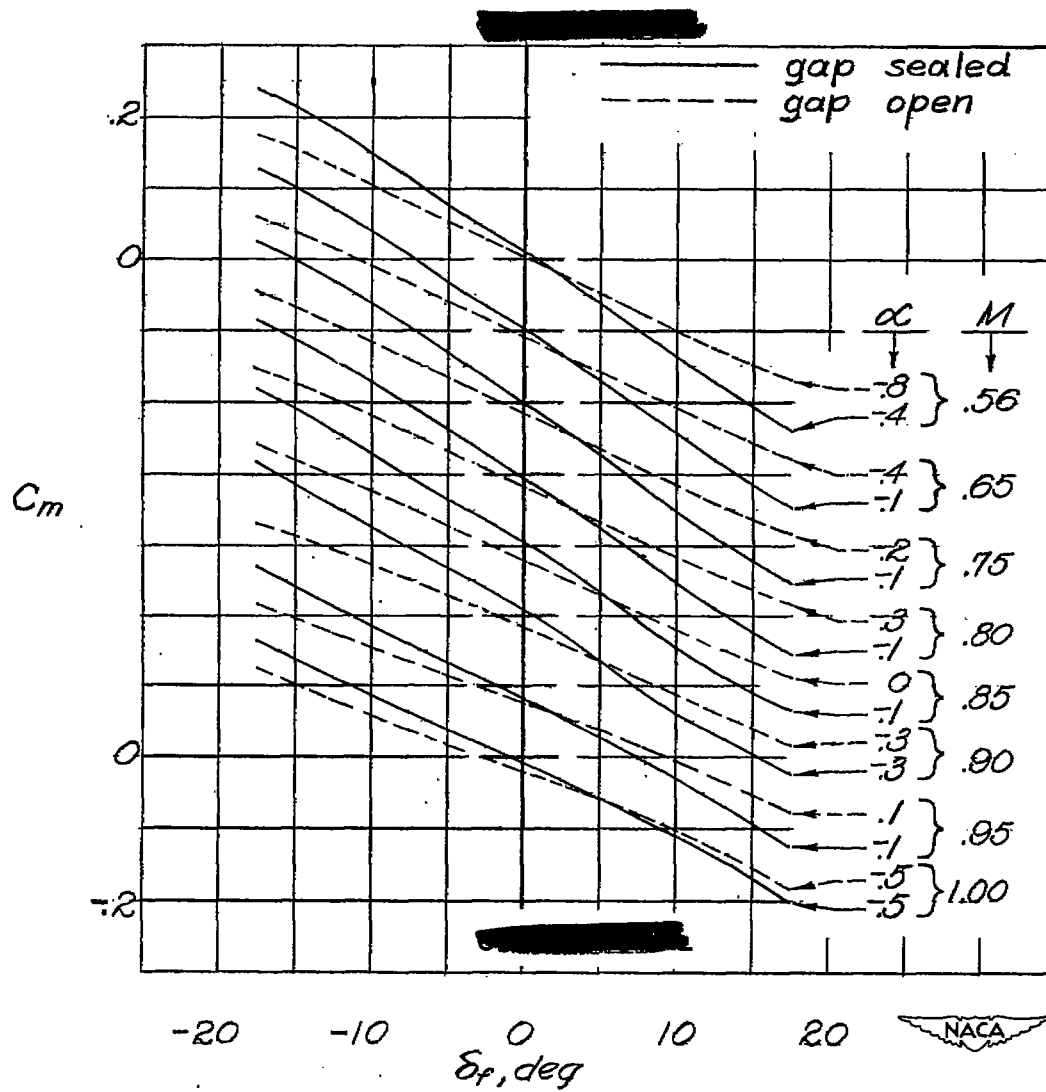
(b) Level-flight runs.

Figure 13.- Concluded.



(a) High-dive runs.

Figure 14.- Variation of pitching-moment coefficient with flap deflection throughout Mach number range tested for $\alpha \approx 0^\circ$. NACA 65-009 airfoil, $A = 3.07$, $\Lambda = 35^\circ$, $c_f = 0.24c$, gap sealed and unsealed, bevelled-trailing-edge flap. Moment coefficient given about axis located 18.1 percent mean aerodynamic chord ahead of leading edge of mean aerodynamic chord. Note shift in axis of ordinate scale for different Mach numbers.



(b) Level-flight runs.

Figure 14.- Concluded.

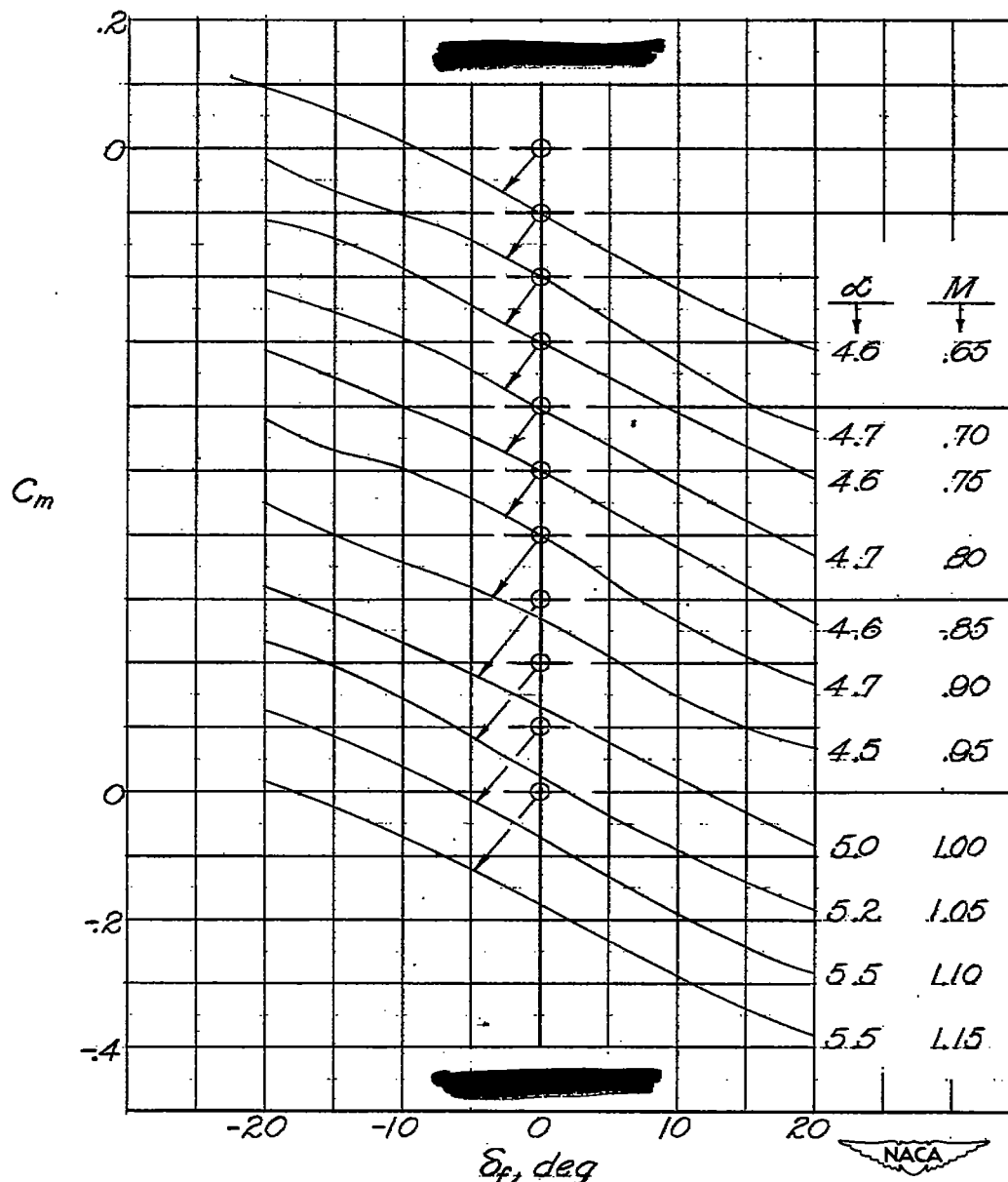
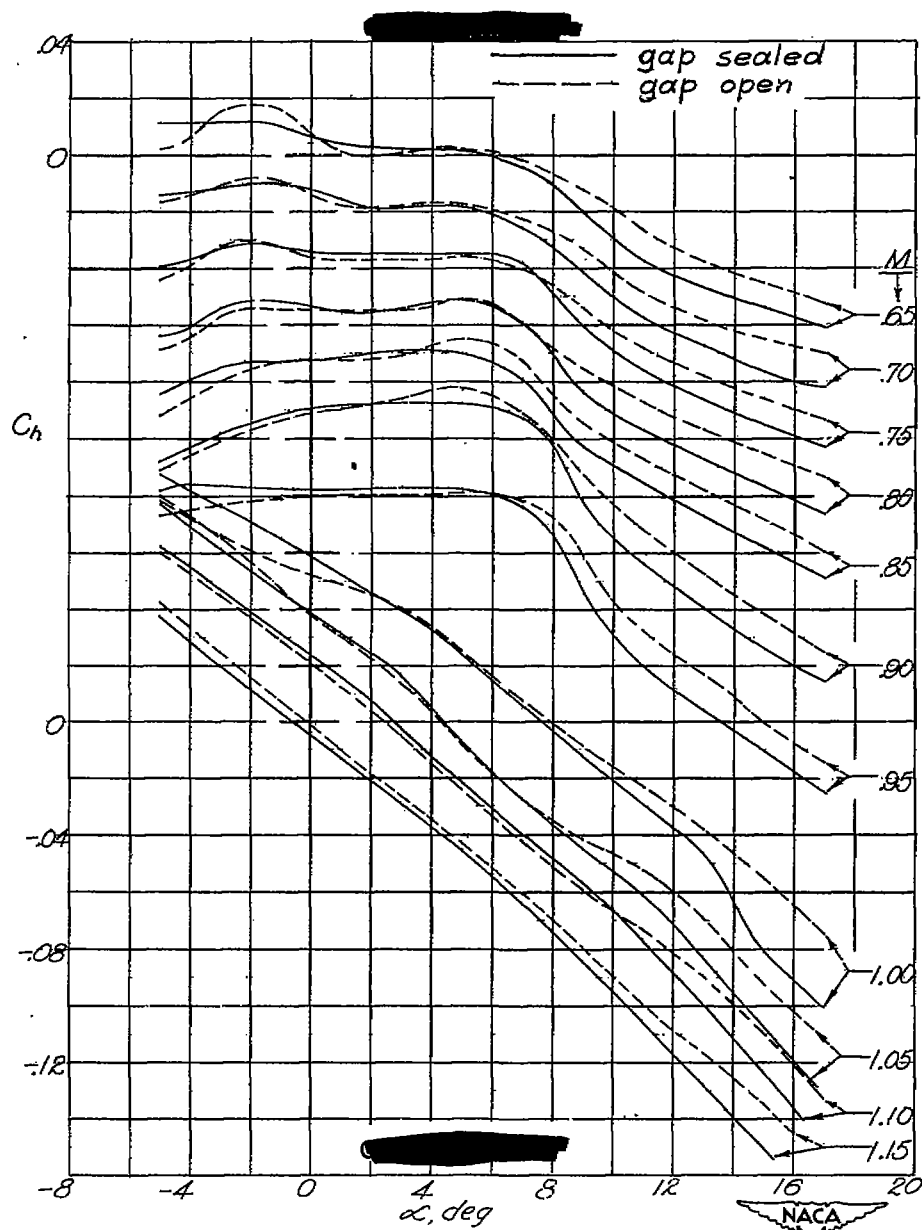
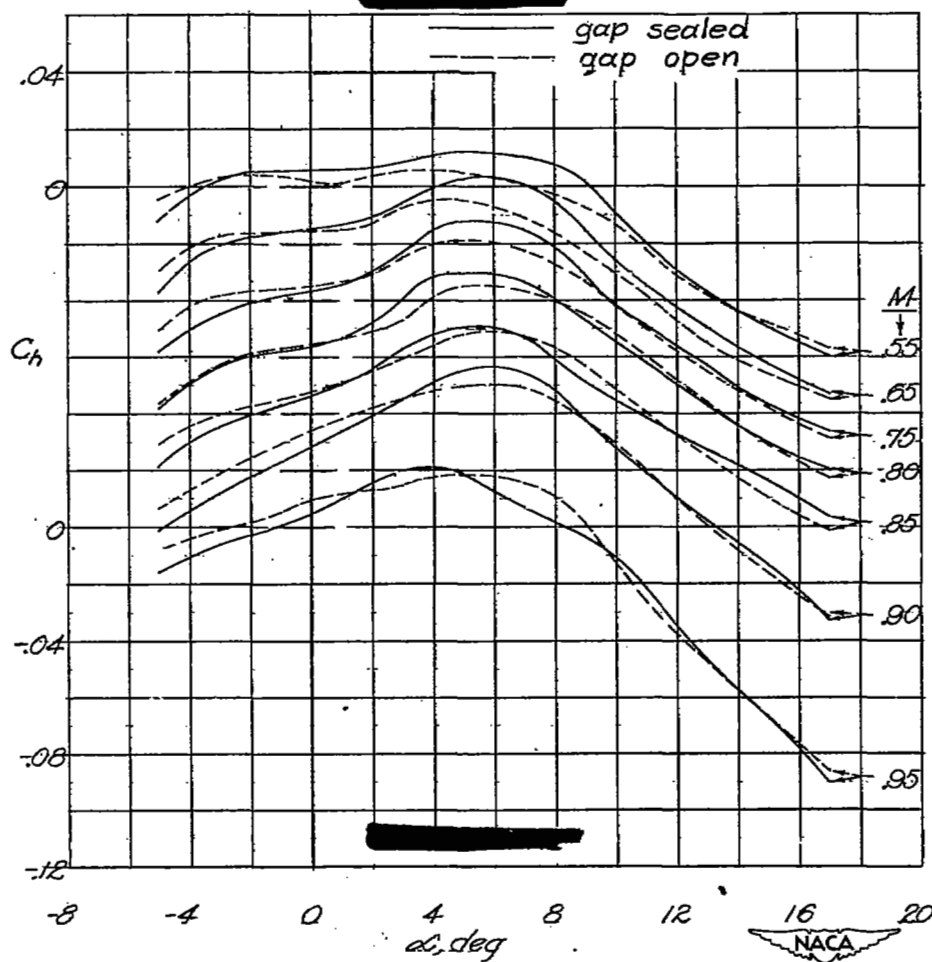


Figure 15.- Variation of pitching-moment coefficient with flap deflection throughout Mach number range tested for $\alpha \approx 5^\circ$. NACA 65-009 airfoil, $A = 3.07$, $\Lambda = 35^\circ$, $c_f = 0.24c$, gap sealed, bevelled-trailing-edge flap. Moment coefficient given about axis located 18.1 percent mean aerodynamic chord ahead of leading edge of mean aerodynamic chord. Note shift in axis of ordinate scale for different Mach numbers. High-dive runs.



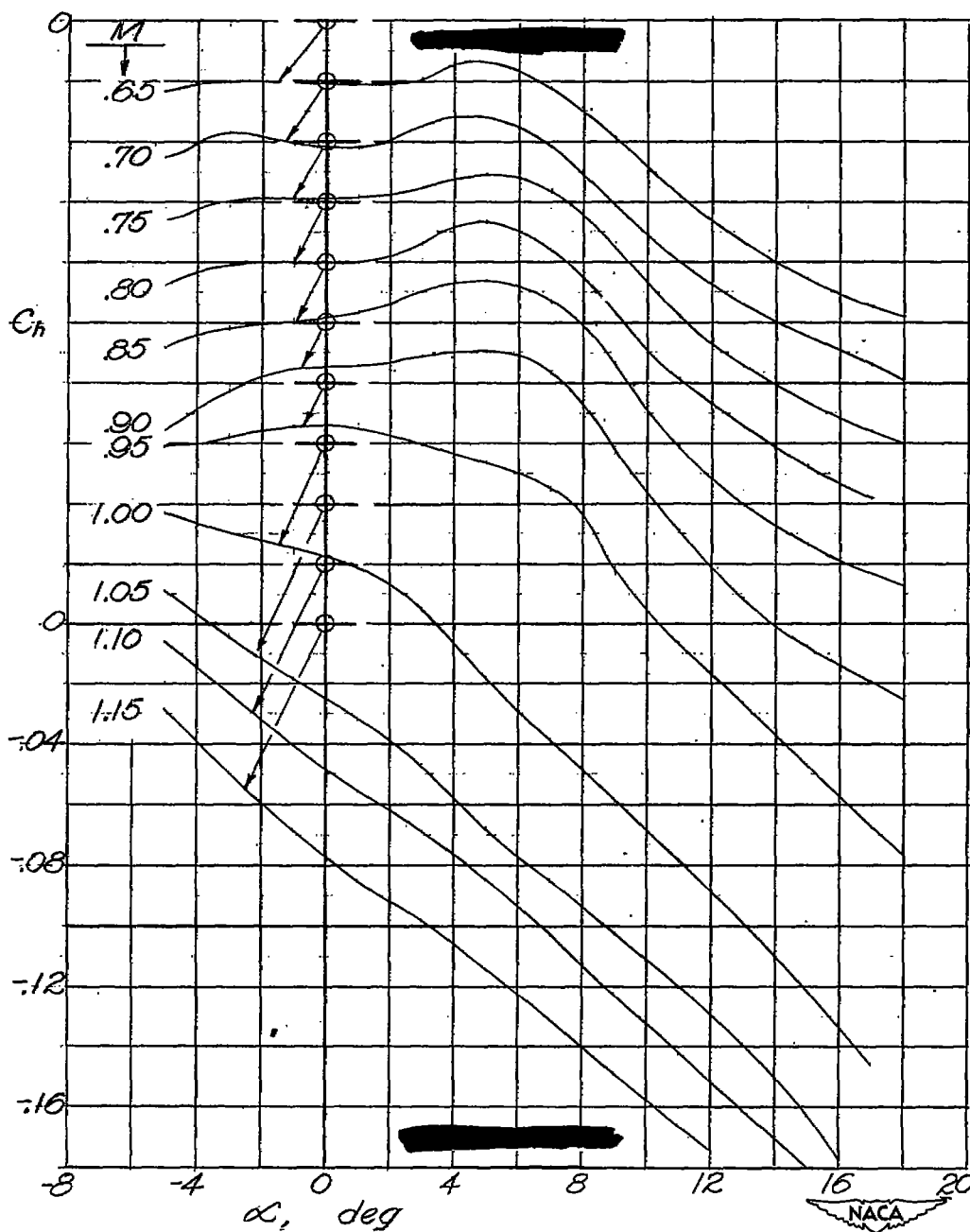
(a) High-dive runs.

Figure 16.- Variation of hinge-moment coefficient with angle of attack throughout Mach number range tested for $\delta_f = 0^\circ$, NACA 65-009 airfoil, $A = 3.07$, $\Lambda = 35^\circ$, $c_f = 0.24c$, gap sealed and unsealed, bevelled-trailing-edge flap. Note shift in axis of ordinate scale for different Mach numbers.



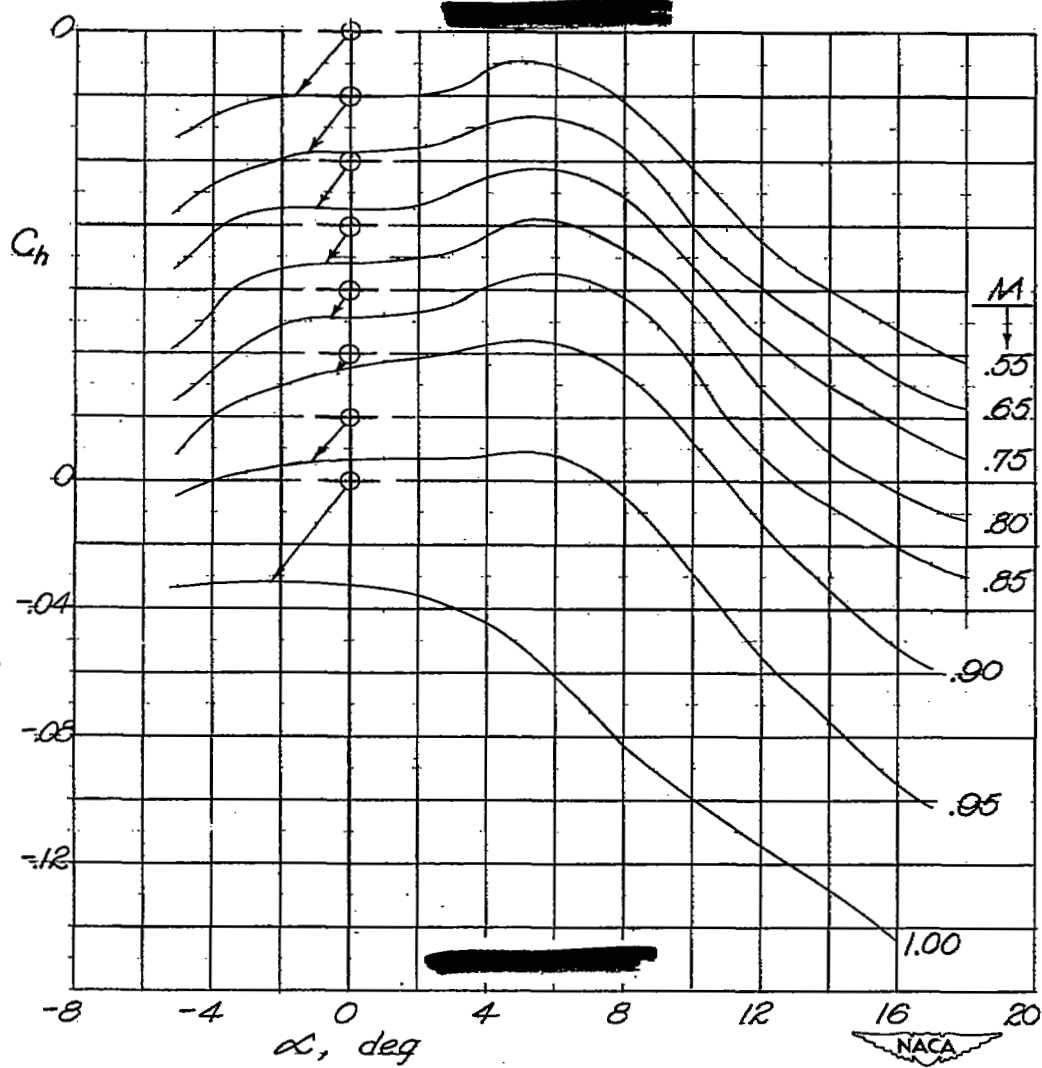
(b) Level-flight runs.

Figure 16.- Concluded.



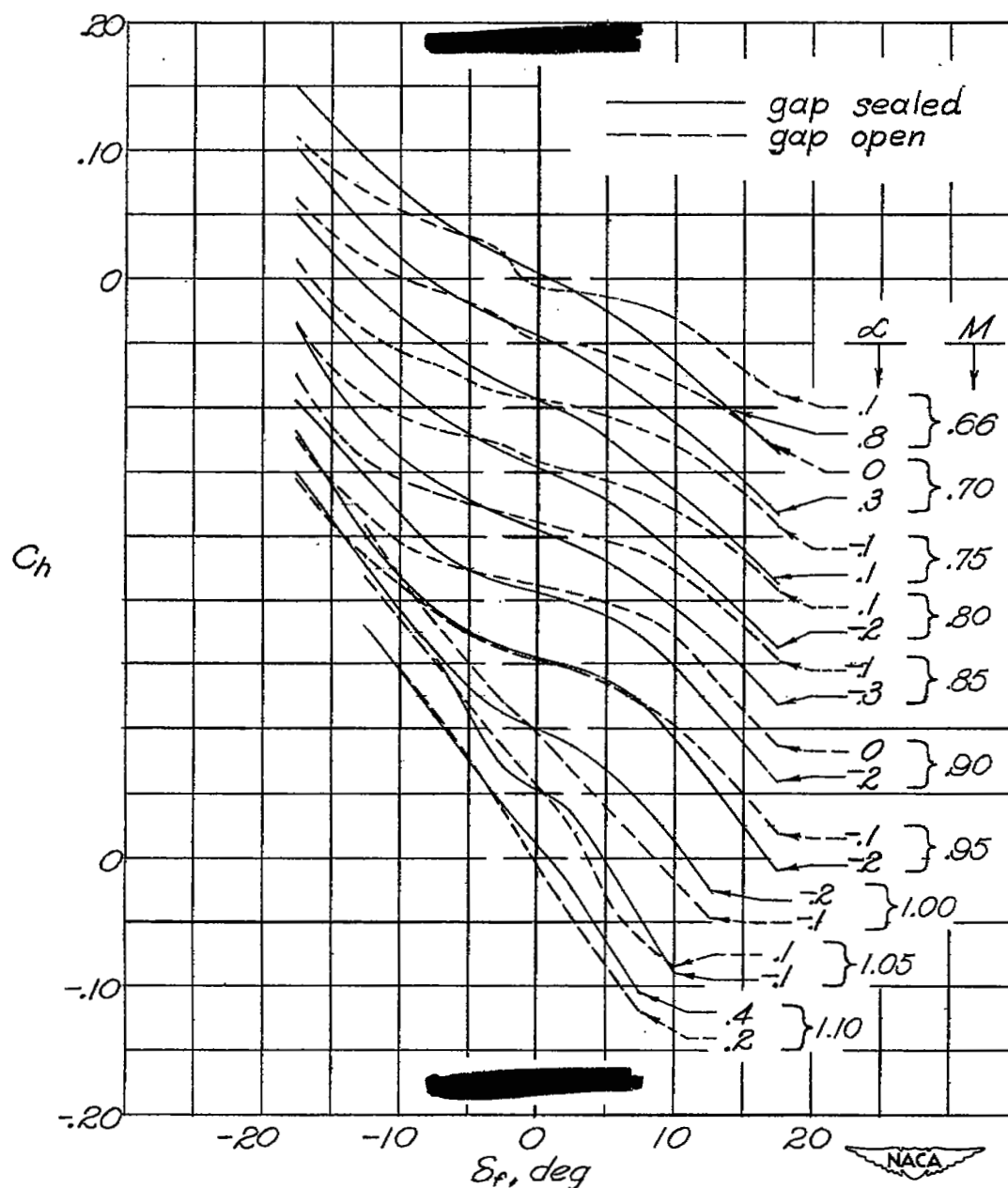
(a) High-dive runs.

Figure 17.- Variation of hinge-moment coefficient with angle of attack throughout Mach number tested for $\delta_f = 5^\circ$. NACA 65-009 airfoil, $A = 3.07$, $\Lambda = 35^\circ$, $c_f = 0.24c$, gap sealed, bevelled-trailing-edge flap. Note shift in axis of ordinate scale for different Mach numbers.



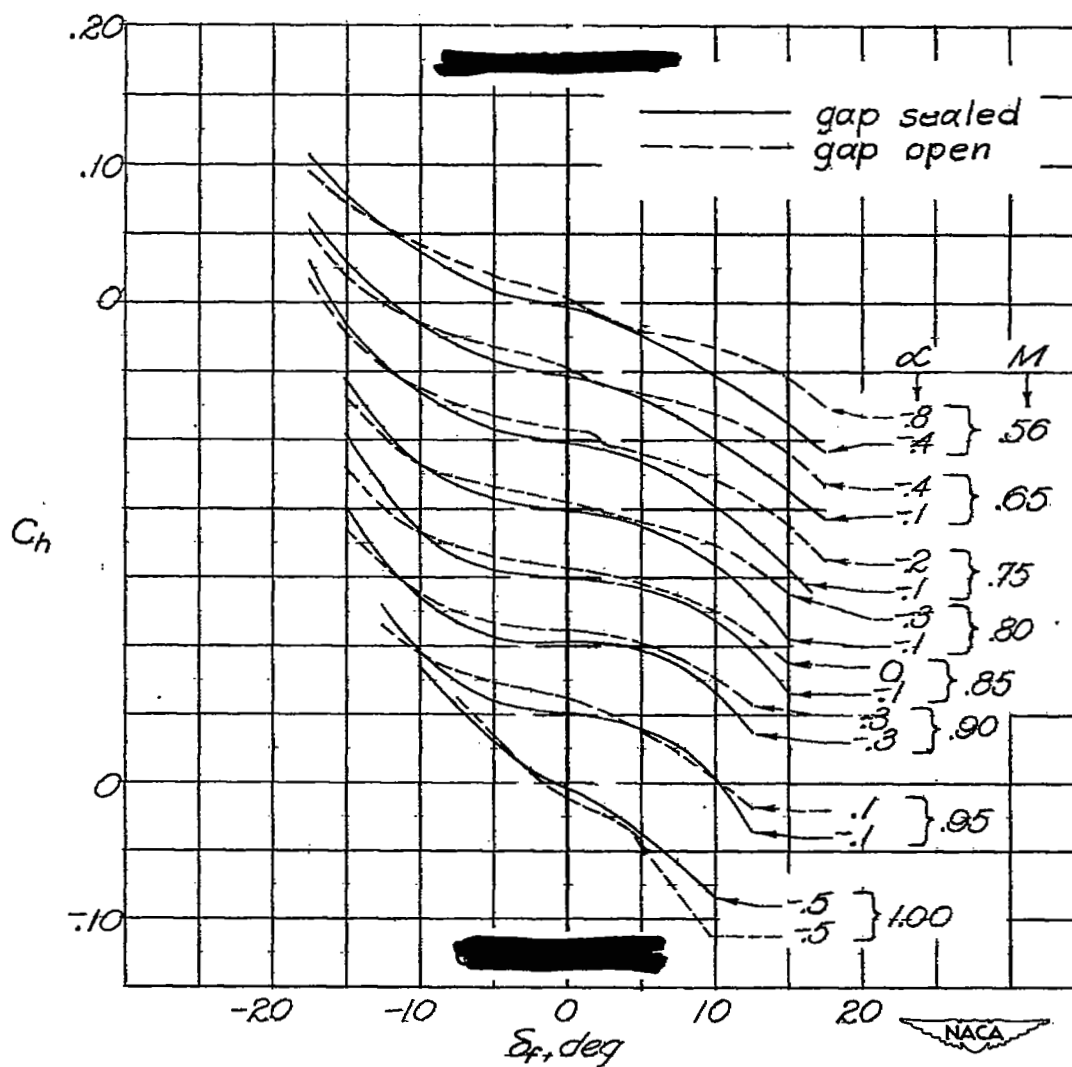
(b) Level-flight runs.

Figure 17.- Concluded.



(a) High-dive runs.

Figure 18.- Variation of hinge-moment coefficient with flap deflection throughout Mach number range tested for $\alpha \approx 0^\circ$. NACA 65-009 airfoil, $A = 3.07$, $\Lambda = 35^\circ$, $c_f = 0.24c$, gap sealed and unsealed, bevelled-trailing-edge flap. Note shift in axis of ordinate scale for different Mach numbers.



(b) Level-flight runs.

Figure 18.- Concluded.

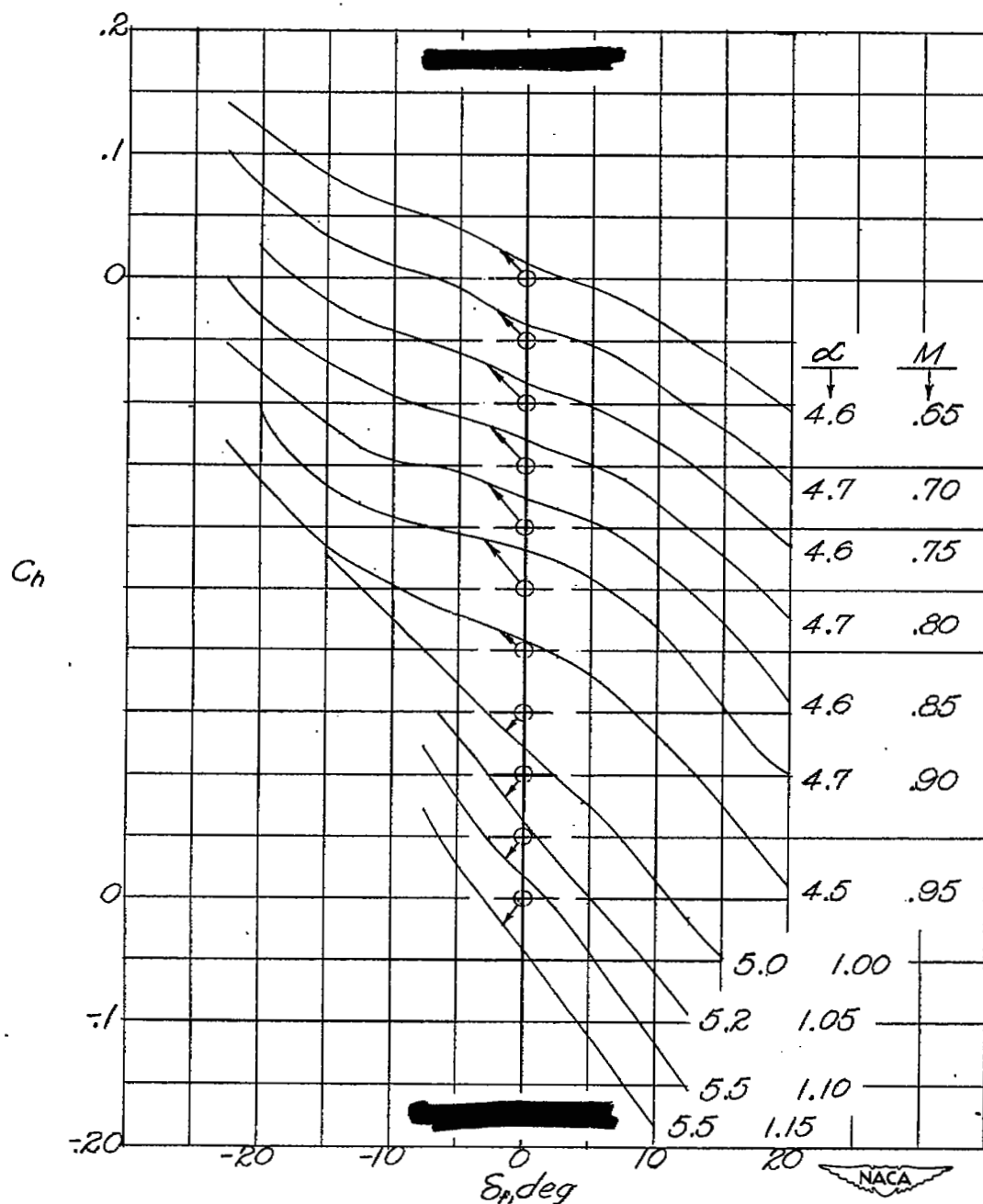


Figure 19.- Variation of hinge-moment coefficient with flap deflection throughout Mach number range tested for $\alpha \approx 5^\circ$. NACA 65-009 airfoil, $A = 3.07$, $\Lambda = 35^\circ$, $c_f = 0.24c$, gap sealed, bevelled-trailing-edge flap. Note shift in axis of ordinate scale for different Mach numbers. High-dive runs.

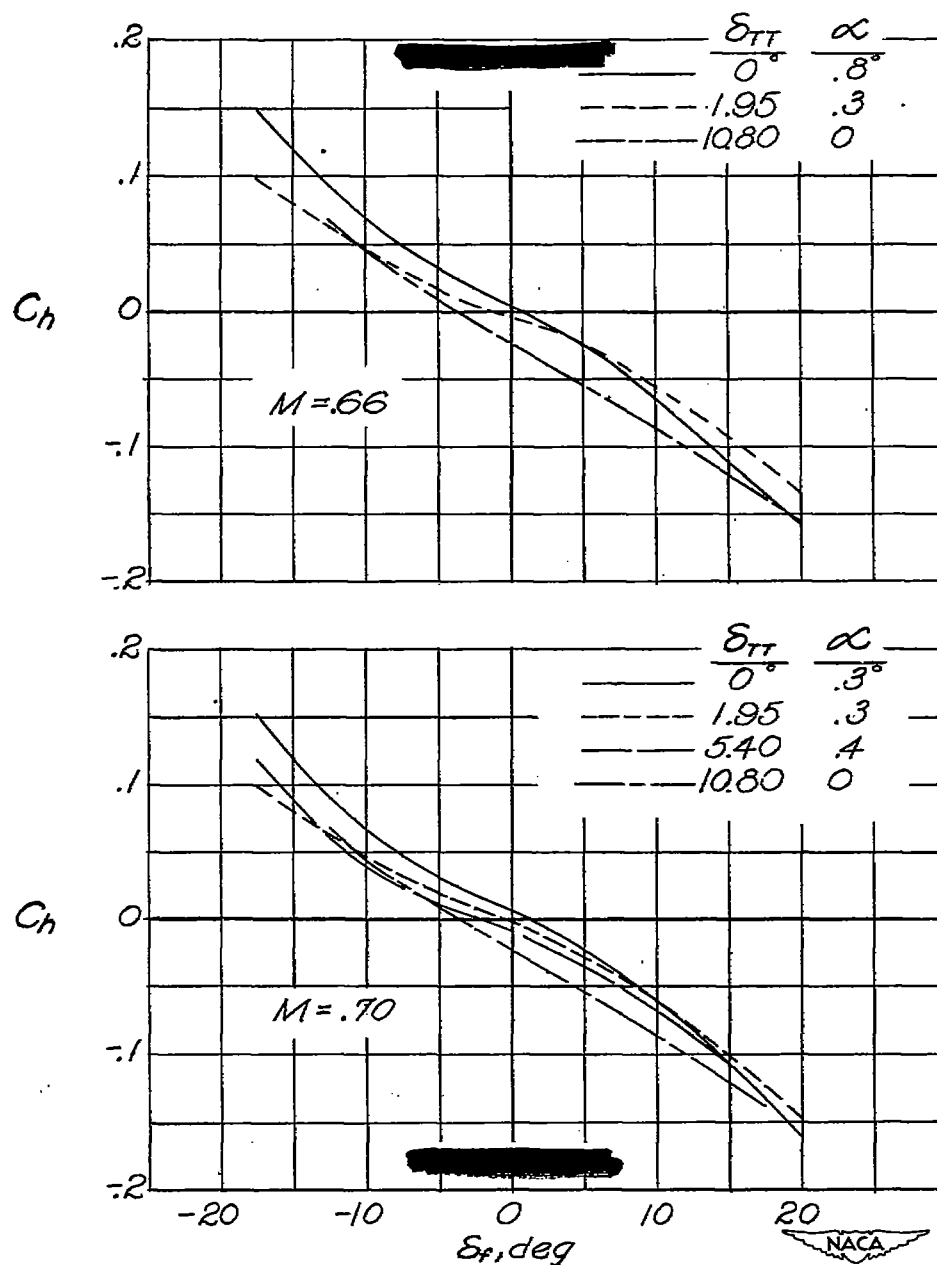
(a) $M = 0.66$ and 0.70 .

Figure 20.- Variation of hinge-moment coefficient with flap deflection for various trim-tab settings throughout Mach number range tested for $\alpha \approx 0^\circ$. NACA 65-009 airfoil, $A = 3.07$, $\Lambda = 35^\circ$, $c_f = 0.24c$, gap sealed, bevelled-trailing-edge flap, $b_{TT} = 0.33b_f$, $c_{TT} = 0.33c_f$. High-dive runs.

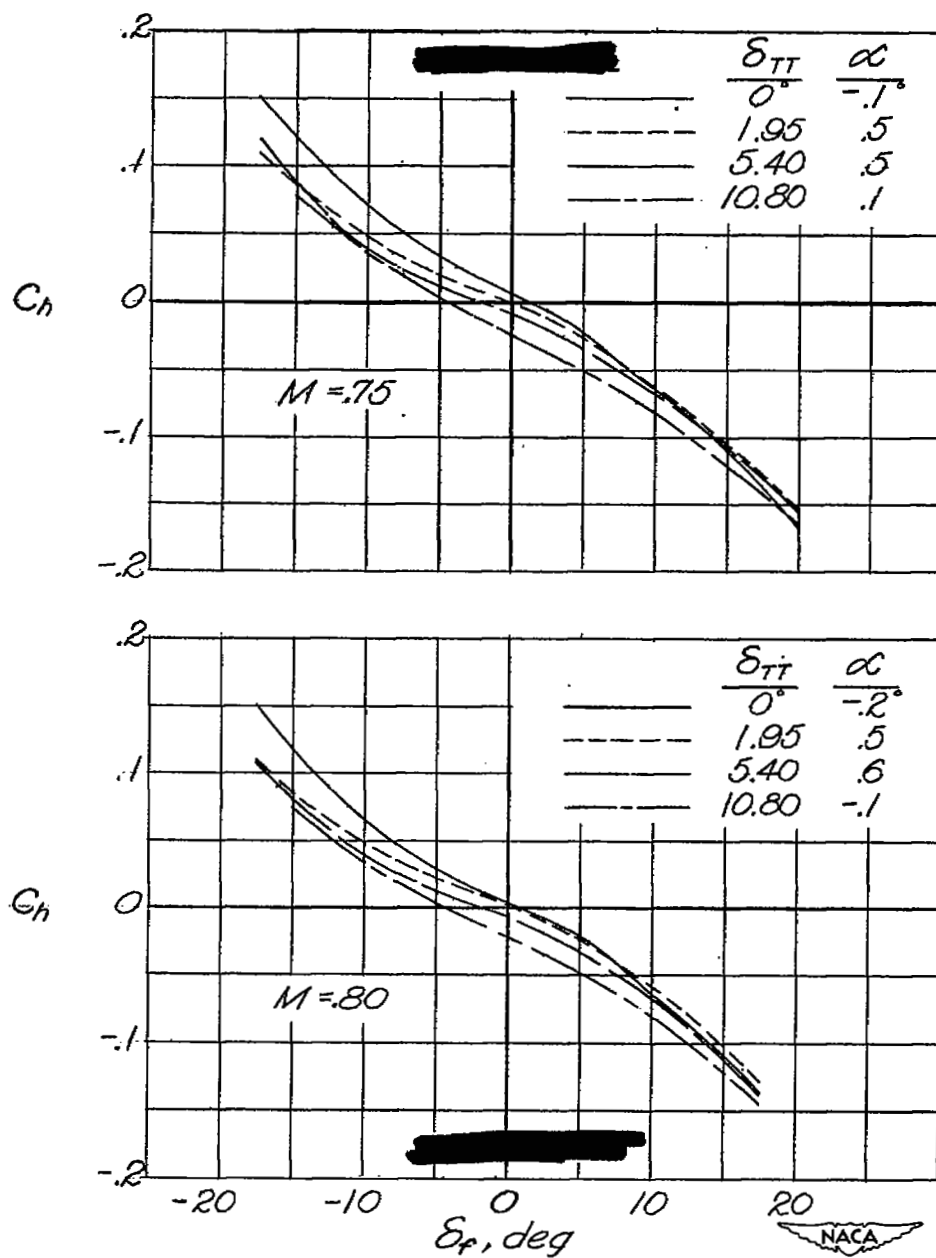
(b) $M = 0.75$ and 0.80 .

Figure 20.- Continued.

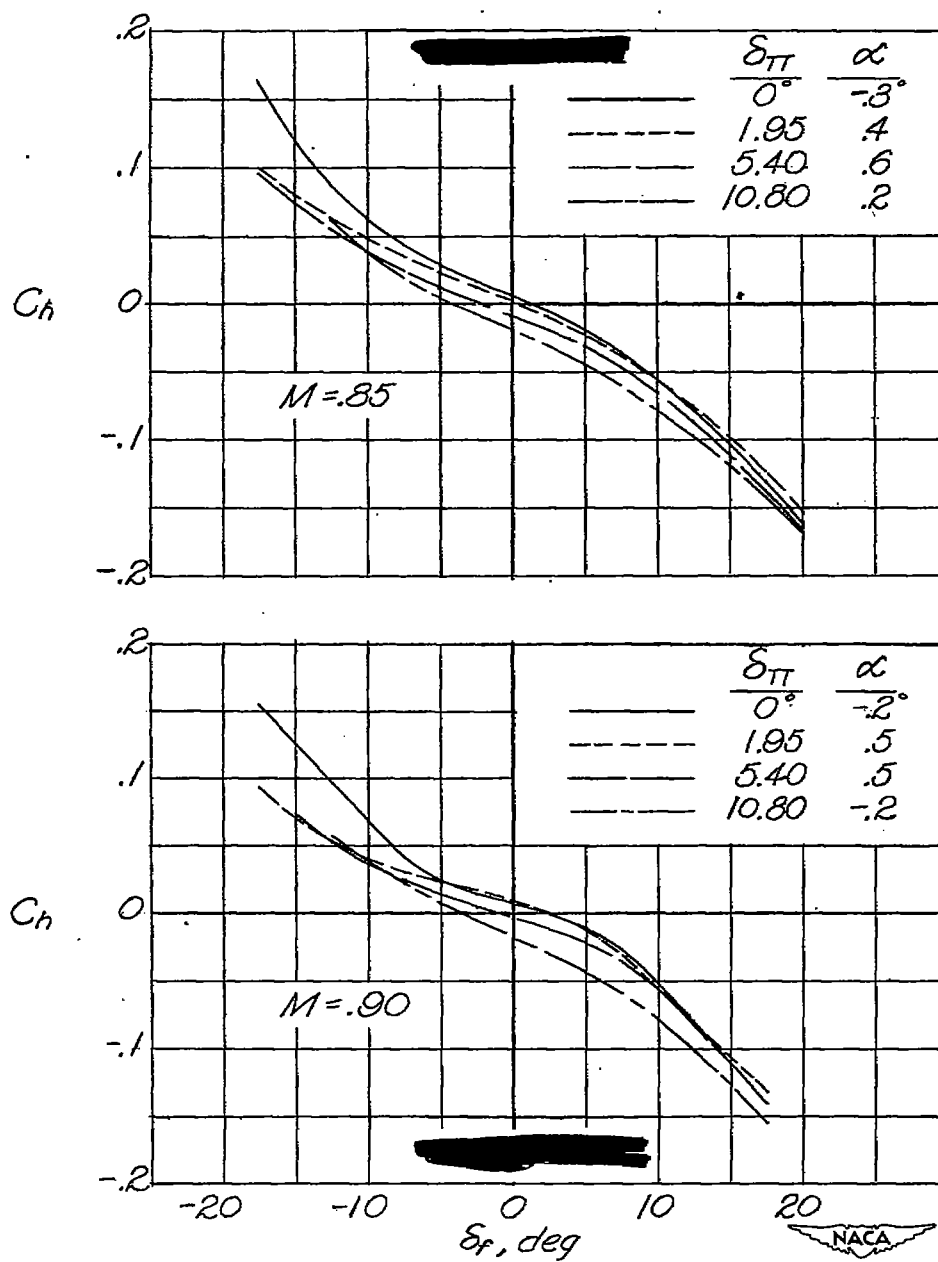
(c) $M = 0.85$ and 0.90 .

Figure 20.- Continued.

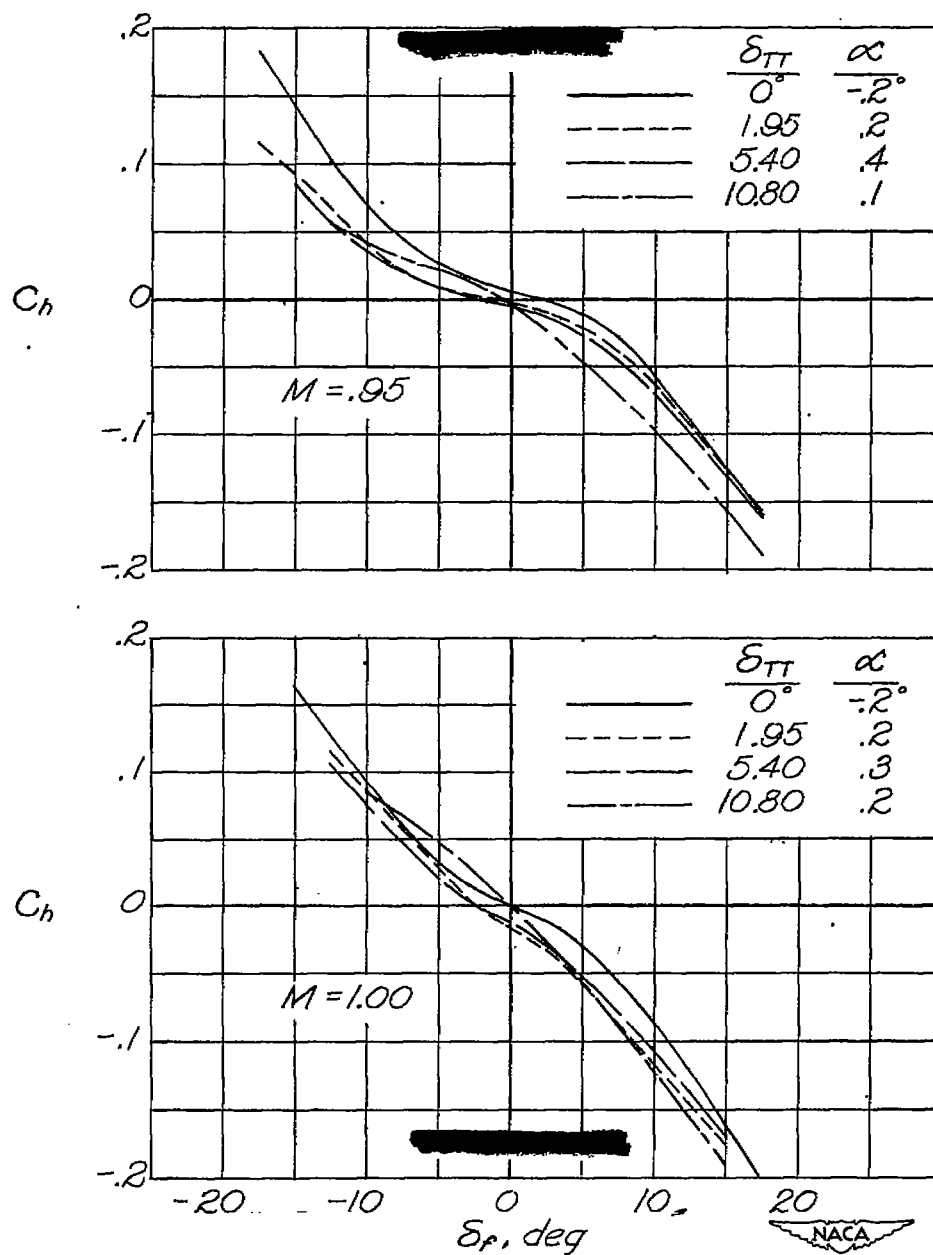
(d) $M = 0.95$ and 1.00 .

Figure 20.- Continued.

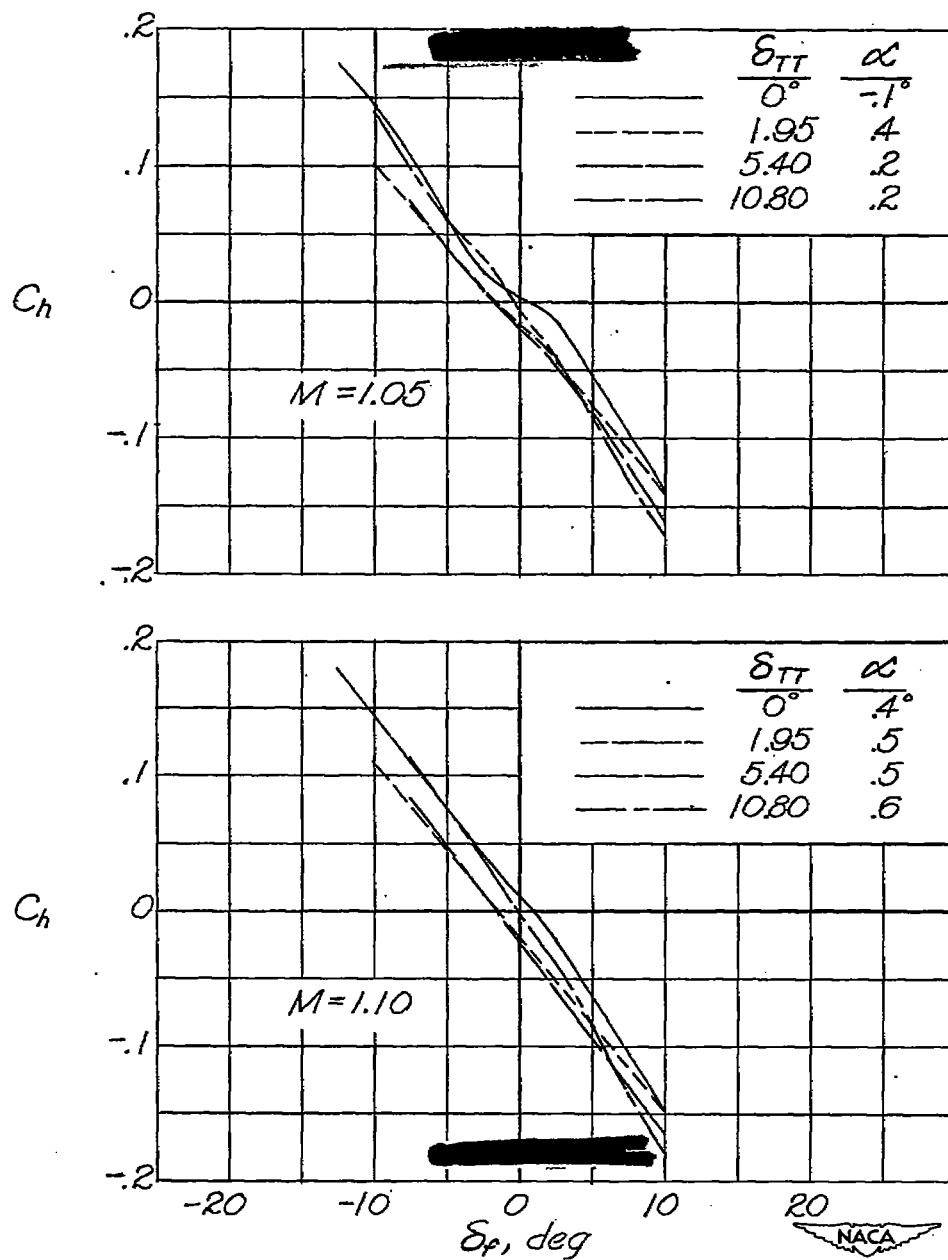
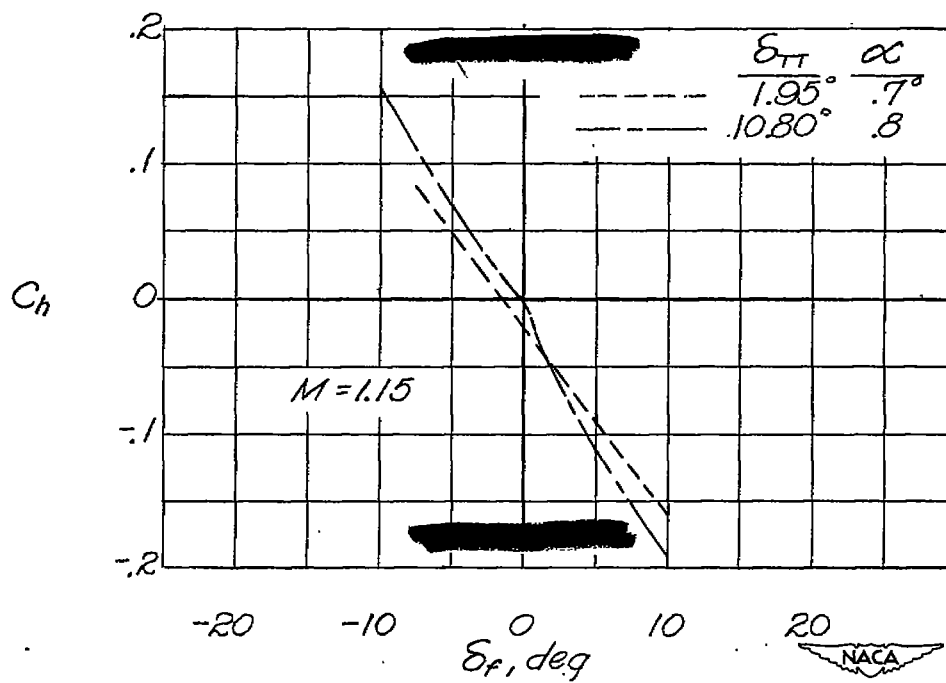
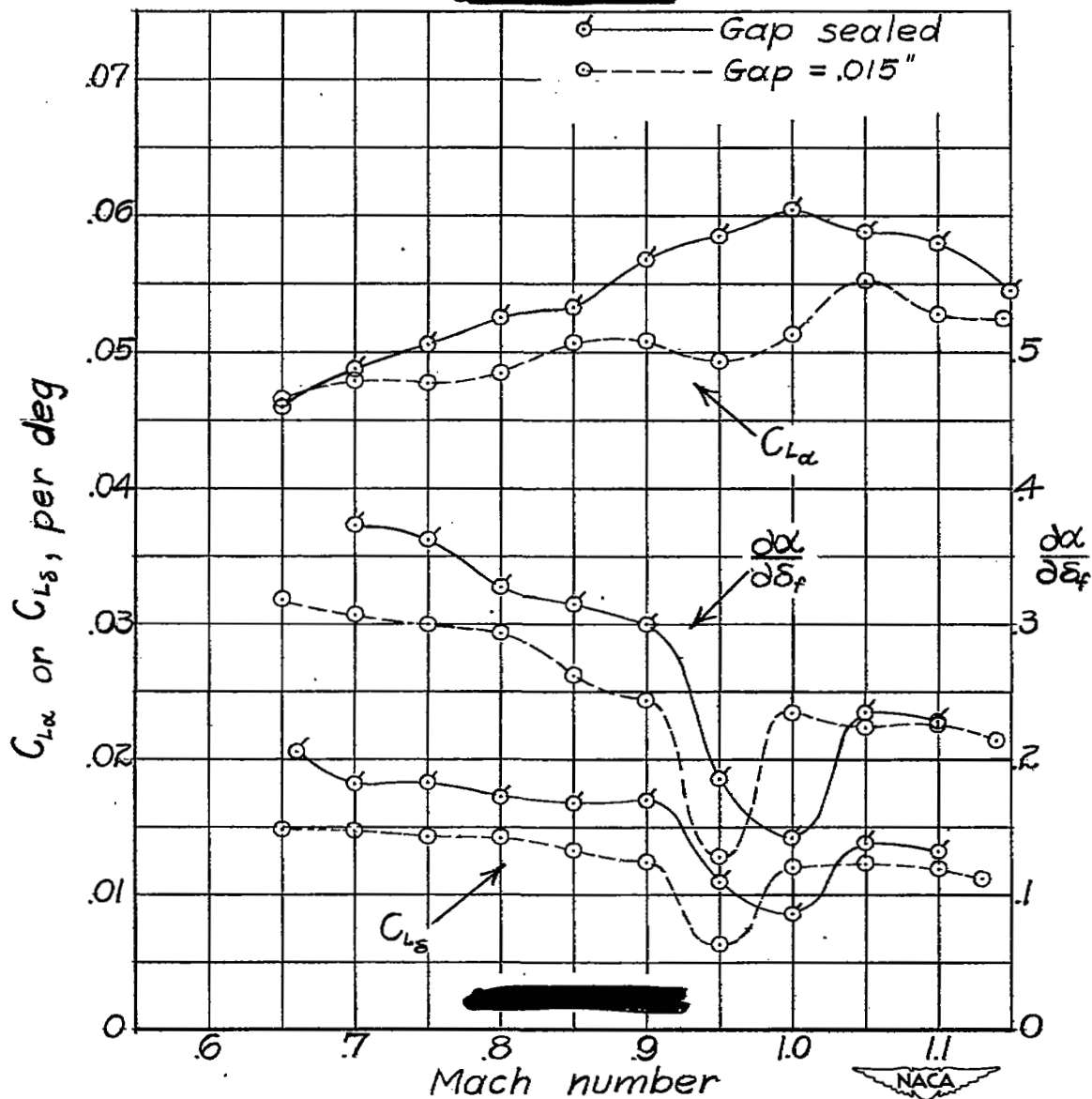
(e) $M = 1.05$ and 1.10 .

Figure 20.- Continued.



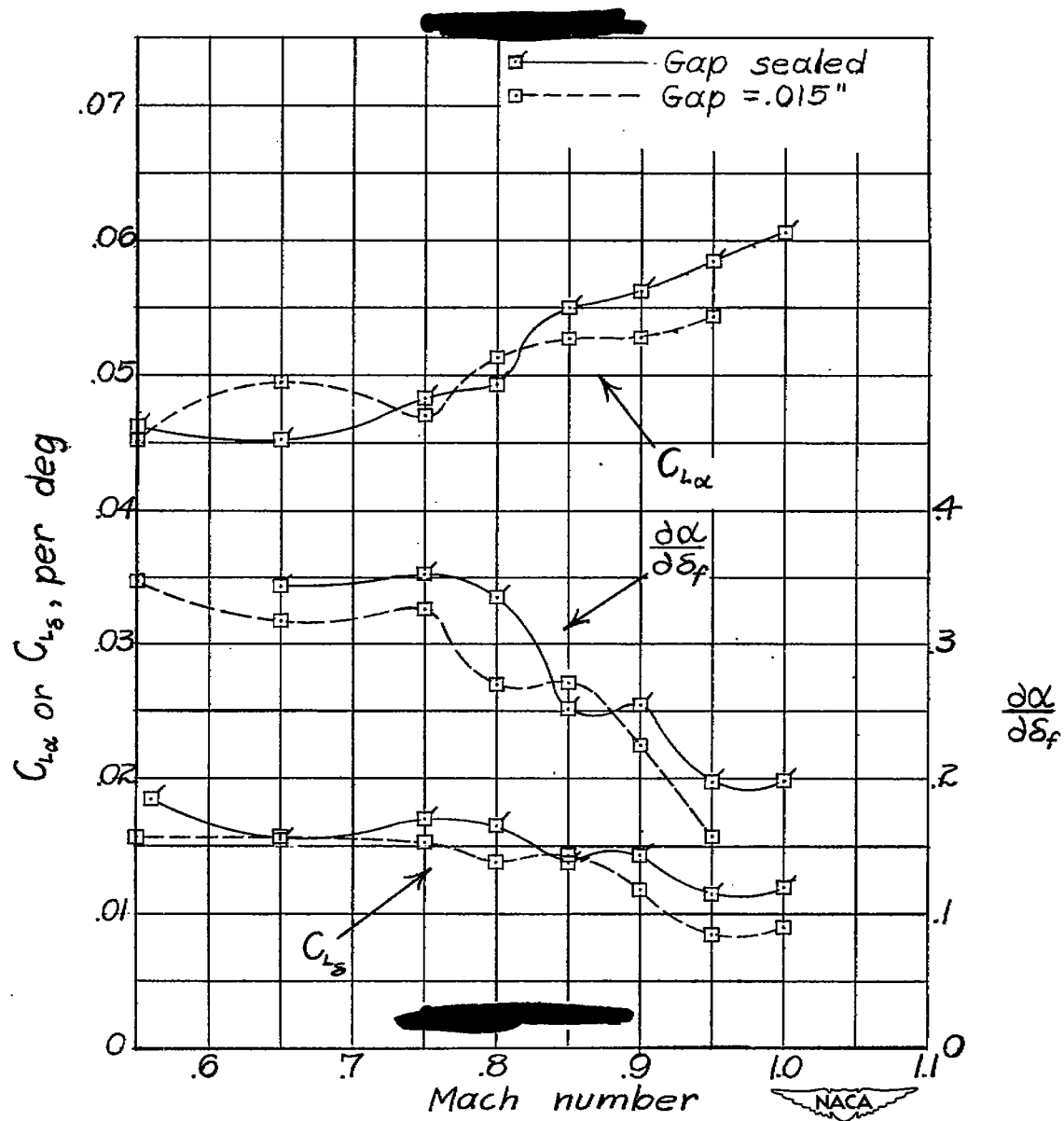
(f) $M = 1.15$.

Figure 20.- Concluded.



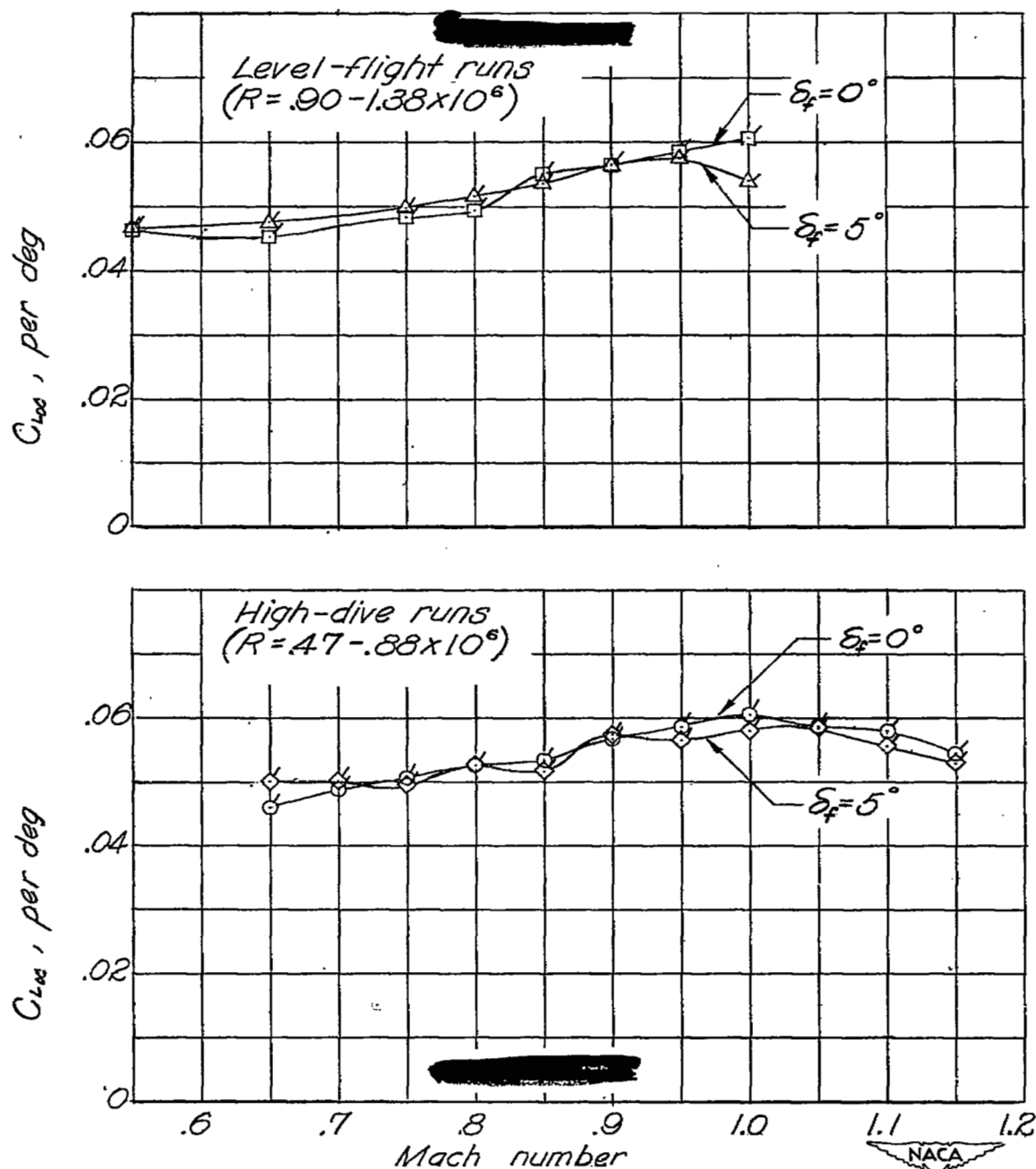
(a) High-dive runs.

Figure 21.- Variation of airfoil model and of flap lift effectiveness with Mach number for $\alpha \approx 0^\circ$, $\delta_f = 0^\circ$. NACA 65-009 airfoil, $A = 3.07$, $\Lambda = 35^\circ$, $c_f = 0.24c$, gap sealed and unsealed, bevelled-trailing-edge flap.



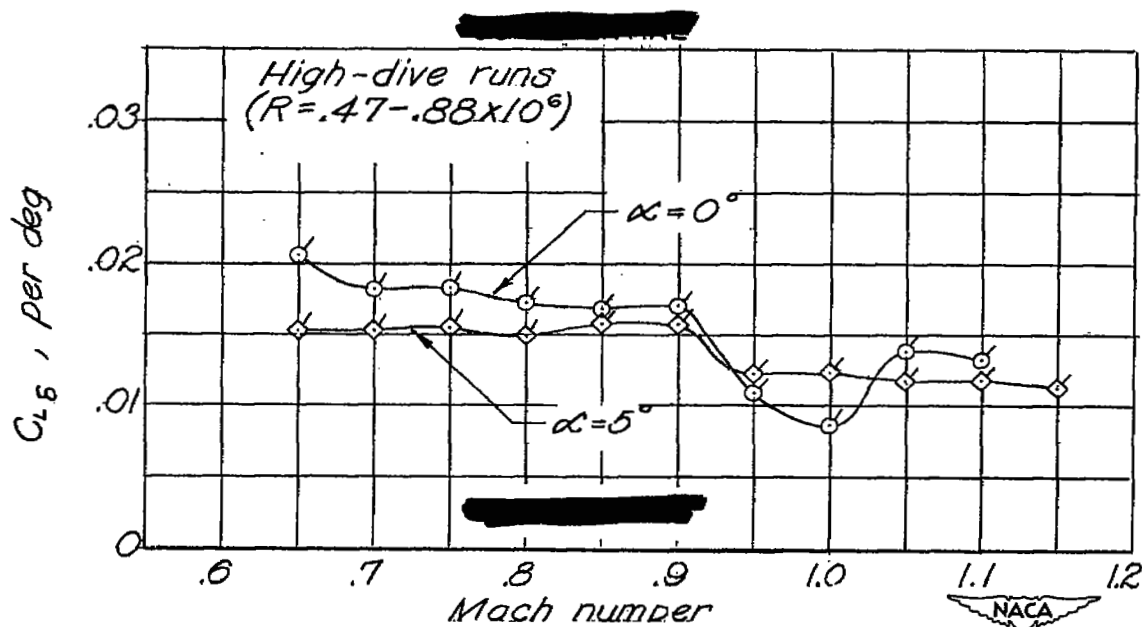
(b) Level-flight runs.

Figure 21.- Concluded.



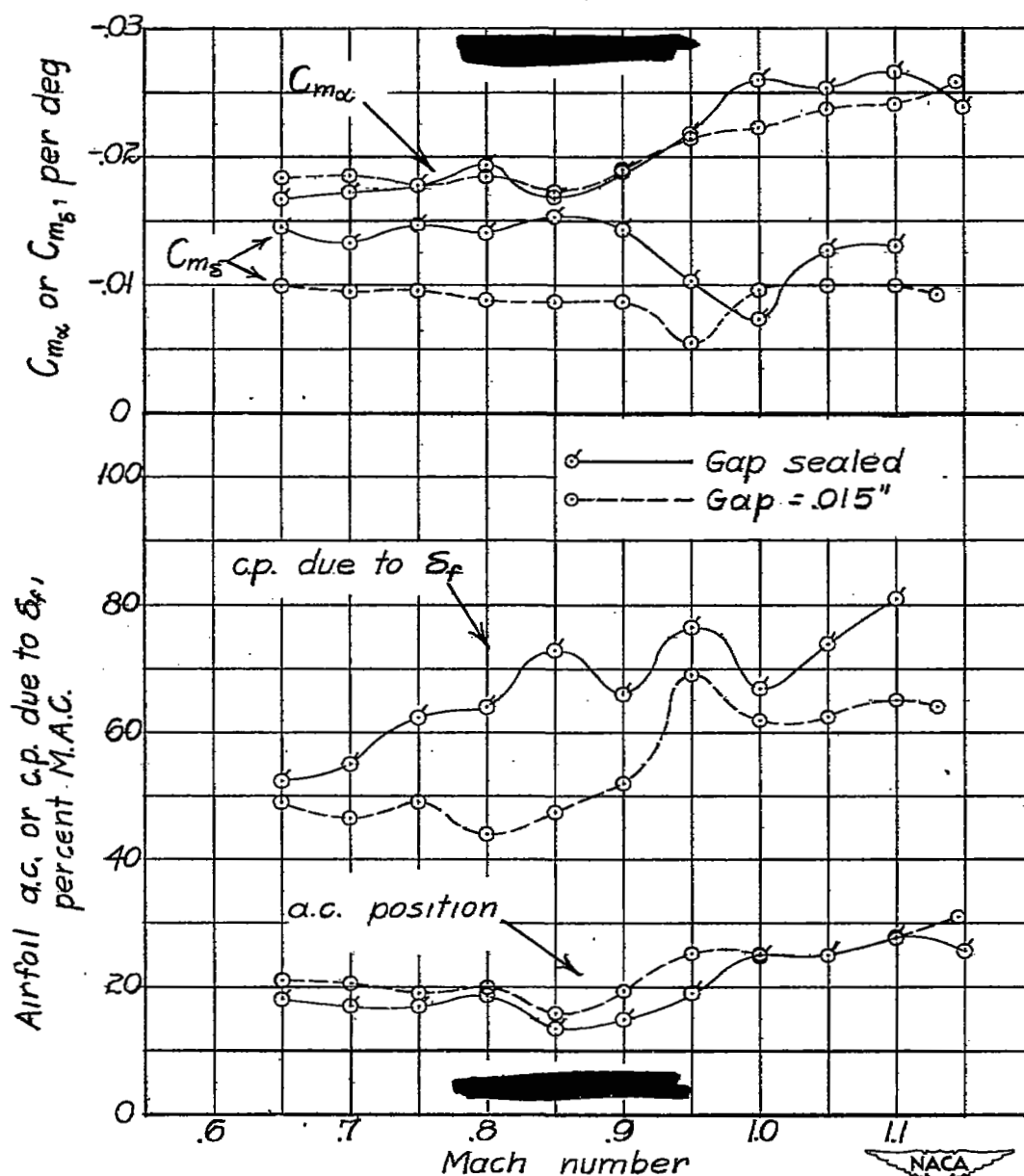
(a) Effect of flap deflection on lift-curve slope at $\alpha = 0^\circ$.

Figure 22.- Effect of flap deflection and angle of attack on airfoil and flap lift effectiveness. NACA 65-009 airfoil, $A = 3.07$, $\Lambda = 35^\circ$, $c_f = 0.24c$, gap sealed, bevelled-trailing-edge flap.



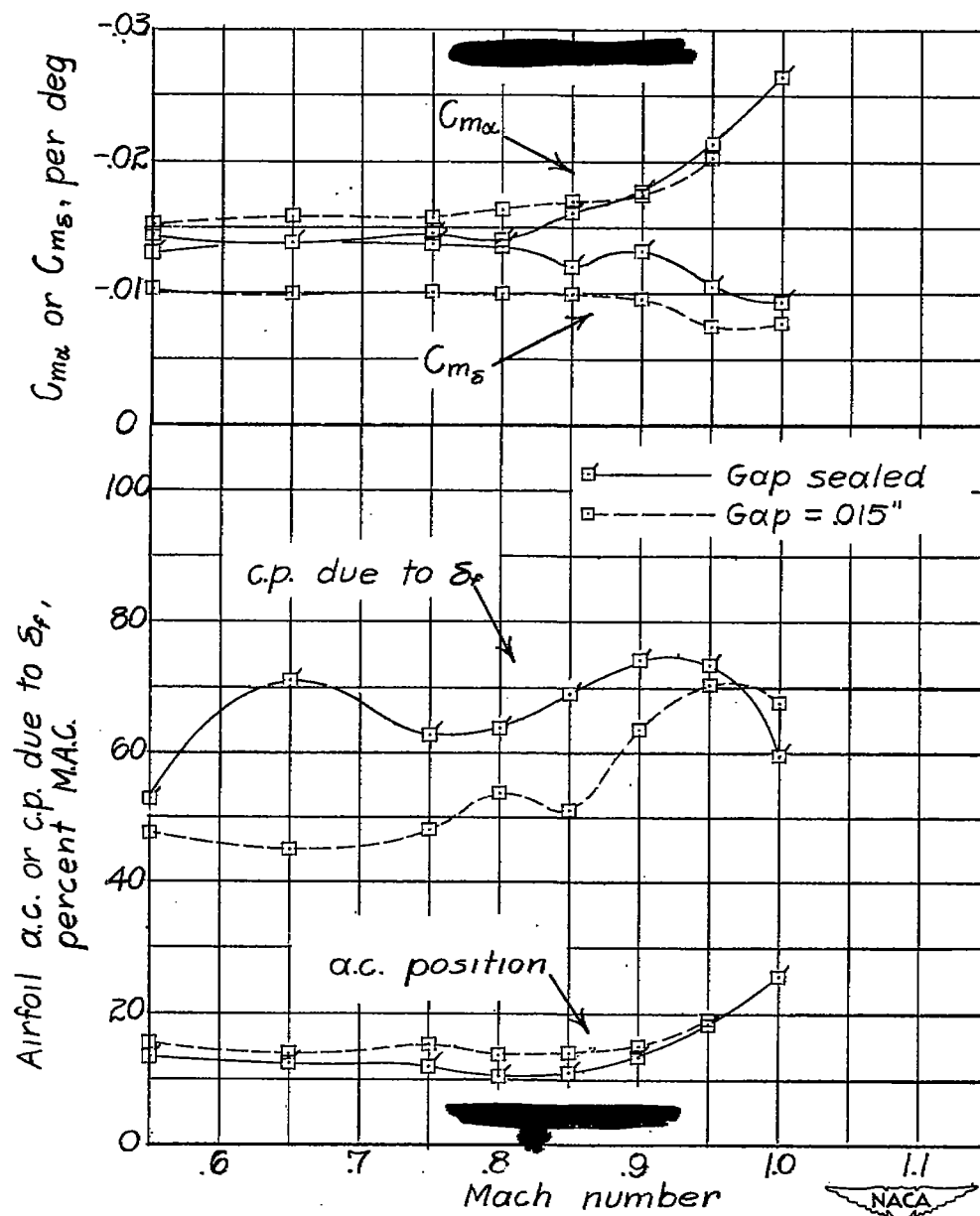
(b) Effect of angle of attack on flap effectiveness at $\delta_f = 0^\circ$.

Figure 22.- Concluded.



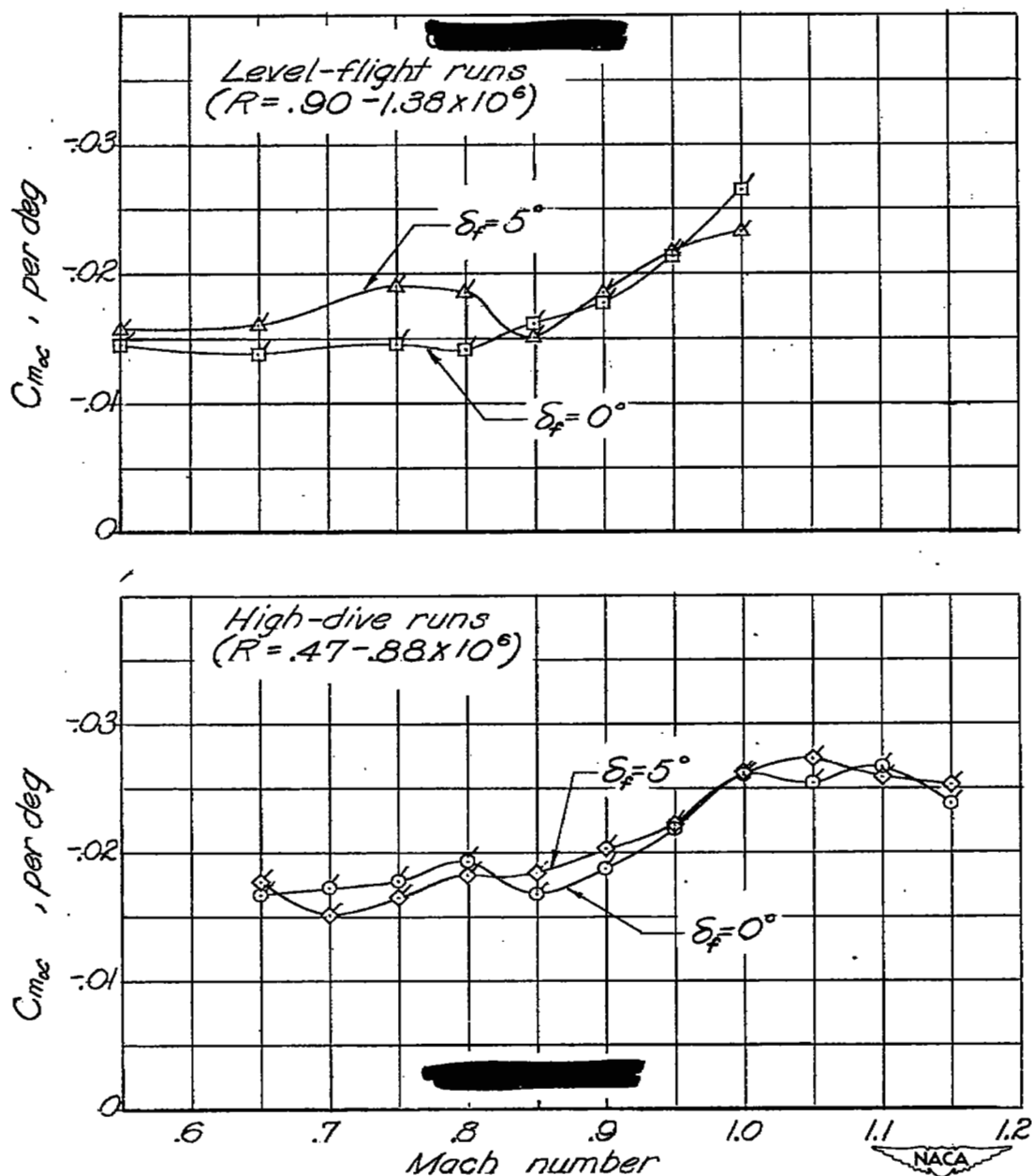
(a) High-dive runs.

Figure 23.- Variation of airfoil model and of flap pitching-moment characteristics with Mach number for $\alpha \approx 0^\circ$, $\delta_f = 0^\circ$. NACA 65-009 airfoil, $A = 3.07$, $\Lambda = 35^\circ$, $c_f = 0.24c$, gap sealed and unsealed, bevelled-trailing-edge flap. Pitching moments measured about axis located 18.1 percent mean aerodynamic chord forward of leading edge of mean aerodynamic chord.



(b) Level-flight runs.

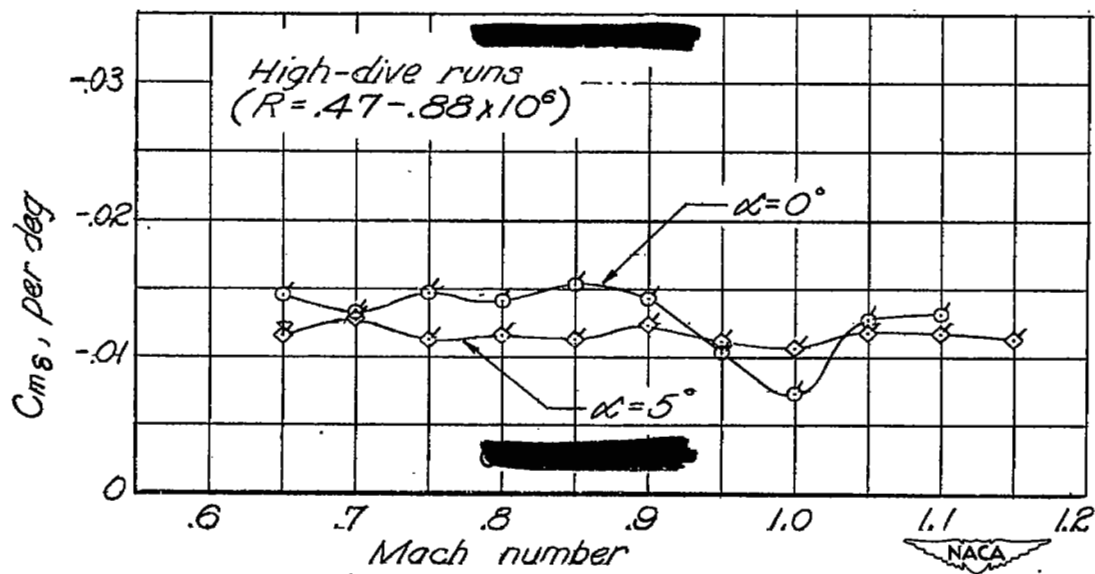
Figure 23.- Concluded.



(a) Effect of flap deflection on airfoil pitching moments at $\alpha \approx 0^\circ$.

Figure 24.- Effect of flap deflection and angle of attack on airfoil and flap pitching-moment characteristics. NACA 65-009 airfoil, $A = 3.07$, $\Lambda = 35^\circ$, $c_f = 0.24c$, gap sealed, bevelled-trailing-edge flap.

Pitching moments measured about axis located 18.1 percent mean aerodynamic chord forward of leading edge of mean aerodynamic chord.



(b) Effect of angle of attack on flap pitching moments at $\delta_f = 0^\circ$.

Figure 24.- Concluded.

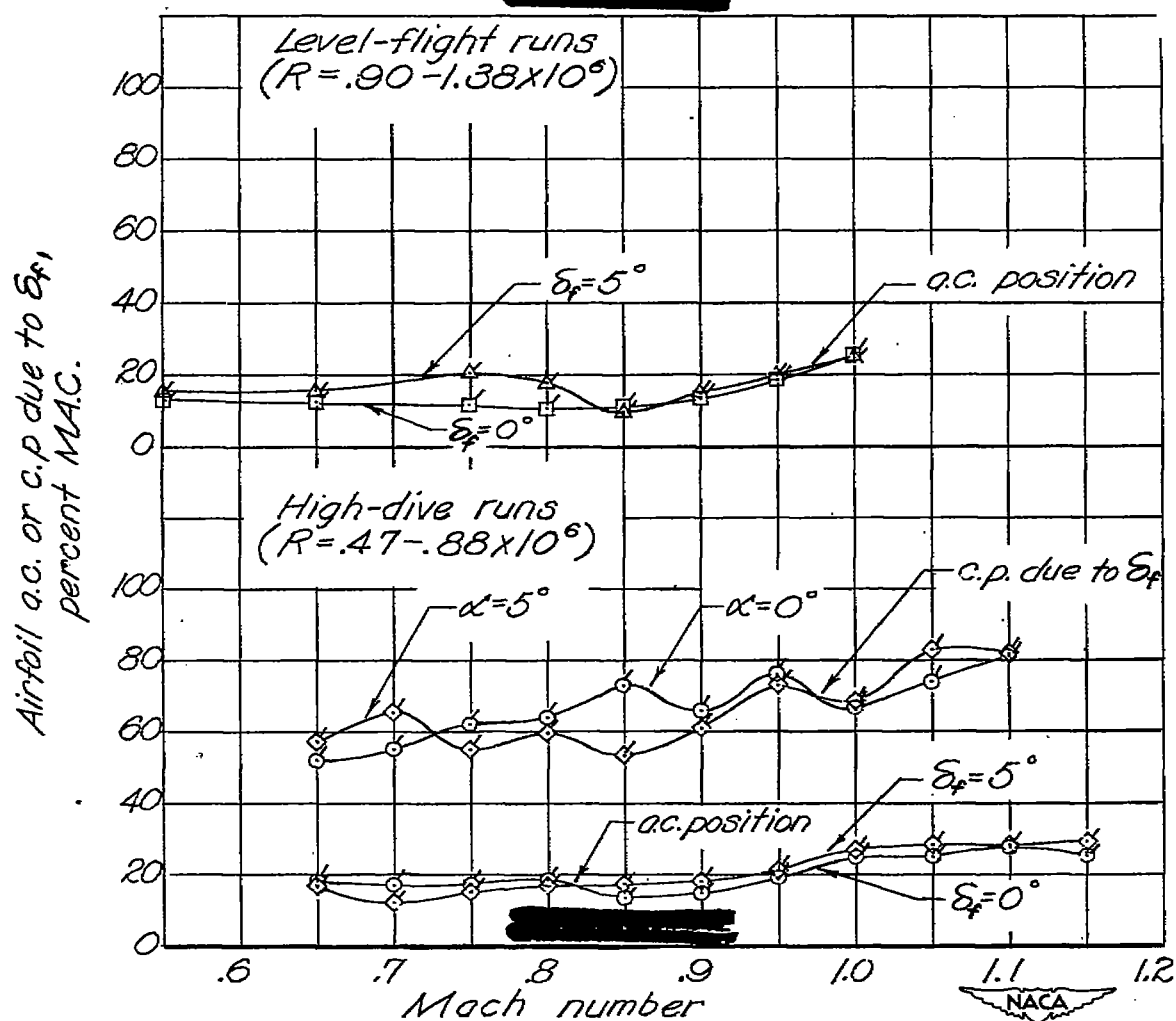


Figure 25.- Effect of angle of attack on center of pressure due to flap deflection and effect of flap deflection on aerodynamic-center location. NACA 65-009 airfoil, $A = 3.07$, $\Lambda = 35^\circ$, $c_f = 0.24c$, gap sealed, bevelled-trailing-edge flap.

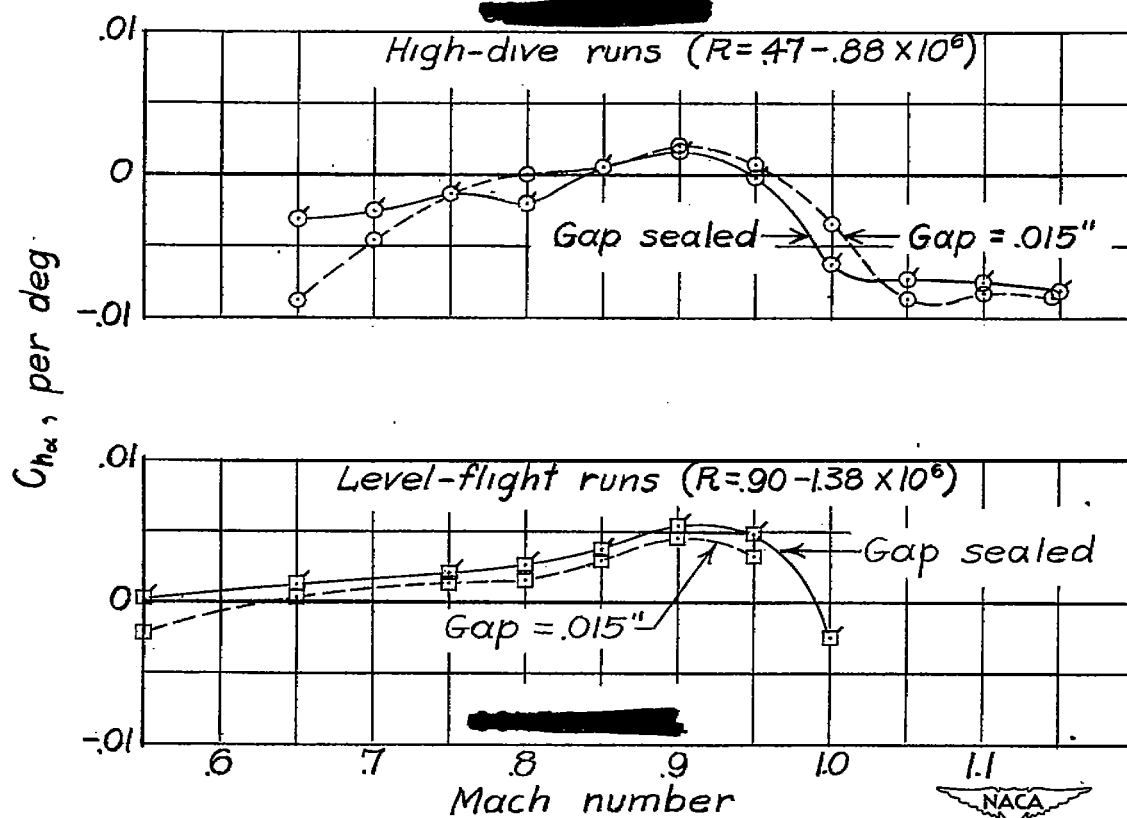


Figure 26.- Variation with Mach number of rate of change of hinge-moment coefficient with change in angle of attack measured at $\alpha \approx 0^\circ$, $\delta_f = 0^\circ$. NACA 65-009 airfoil, $A = 3.07$, $\Lambda = 35^\circ$, $c_f = 0.24c$, gap sealed and unsealed, bevelled-trailing-edge flap.

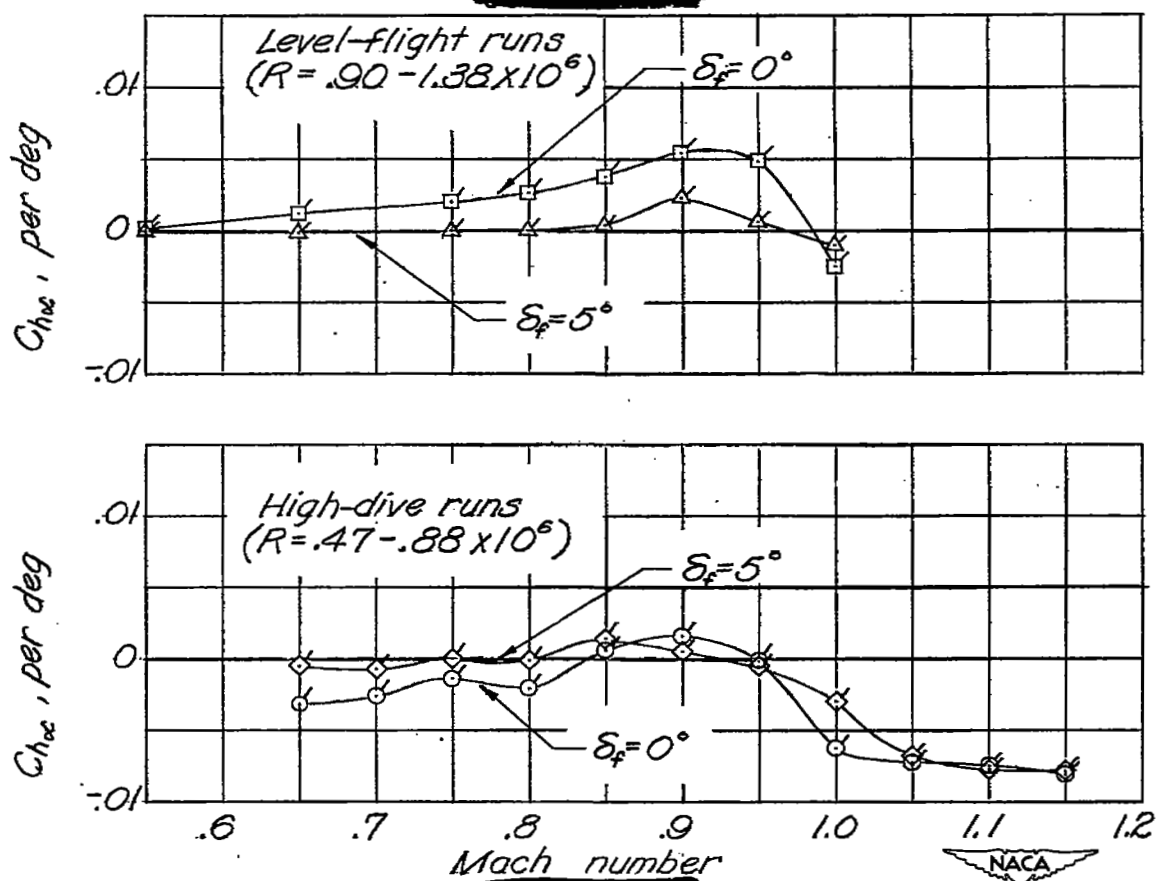


Figure 27.- Effect of flap deflection on rate of change of hinge-moment coefficient with angle of attack measured at $\alpha = 0^\circ$.
NACA 65-009 airfoil, $A = 3.07$, $\Lambda = 35^\circ$, $c_f = 0.24c$, gap sealed, bevelled-trailing-edge flap.

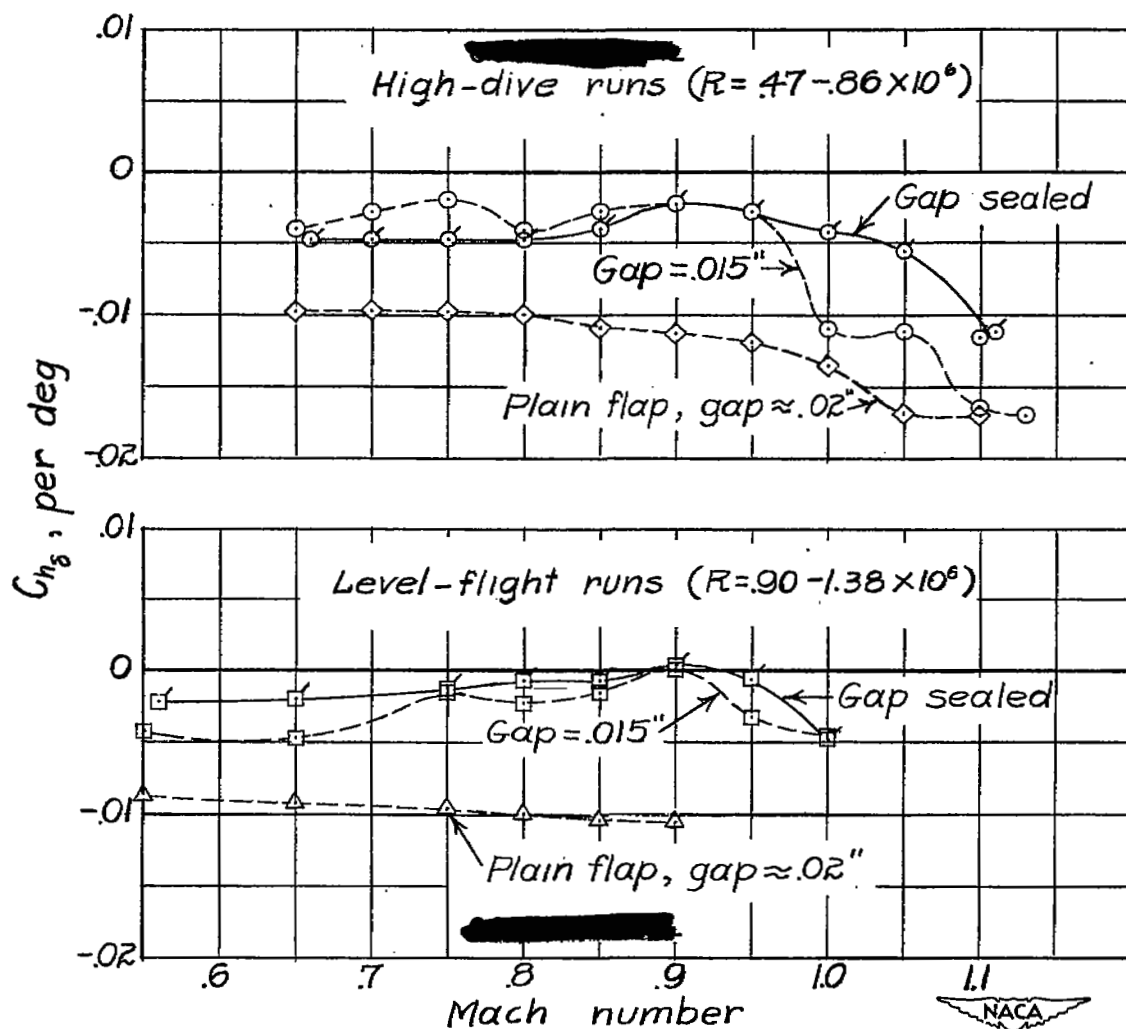


Figure 28.- Variation with Mach number of rate of change of hinge-moment coefficient with change in flap deflection measured at $\alpha \approx 0^\circ$, $\delta_f = 0^\circ$. NACA 65-009 airfoil, $A = 3.07$, $\Lambda = 35^\circ$, $c_f = 0.24c$, gap sealed and unsealed, bevelled-trailing-edge flap. Plain-flap data from reference 1 included for comparison.

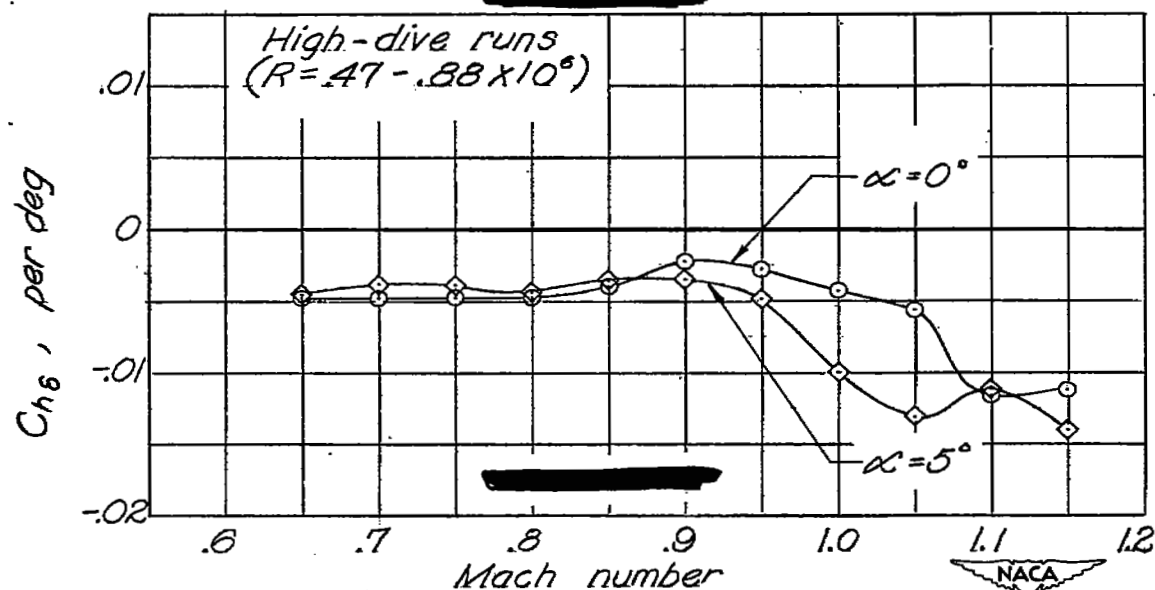


Figure 29.- Effect of angle of attack on rate of change of hinge-moment coefficient with flap deflection measured at $\delta_f = 0^\circ$.
NACA 65-009 airfoil, $A = 3.07$, $\Lambda = 35^\circ$, $c_f = 0.24c$, gap sealed, bevelled-trailing-edge flap.

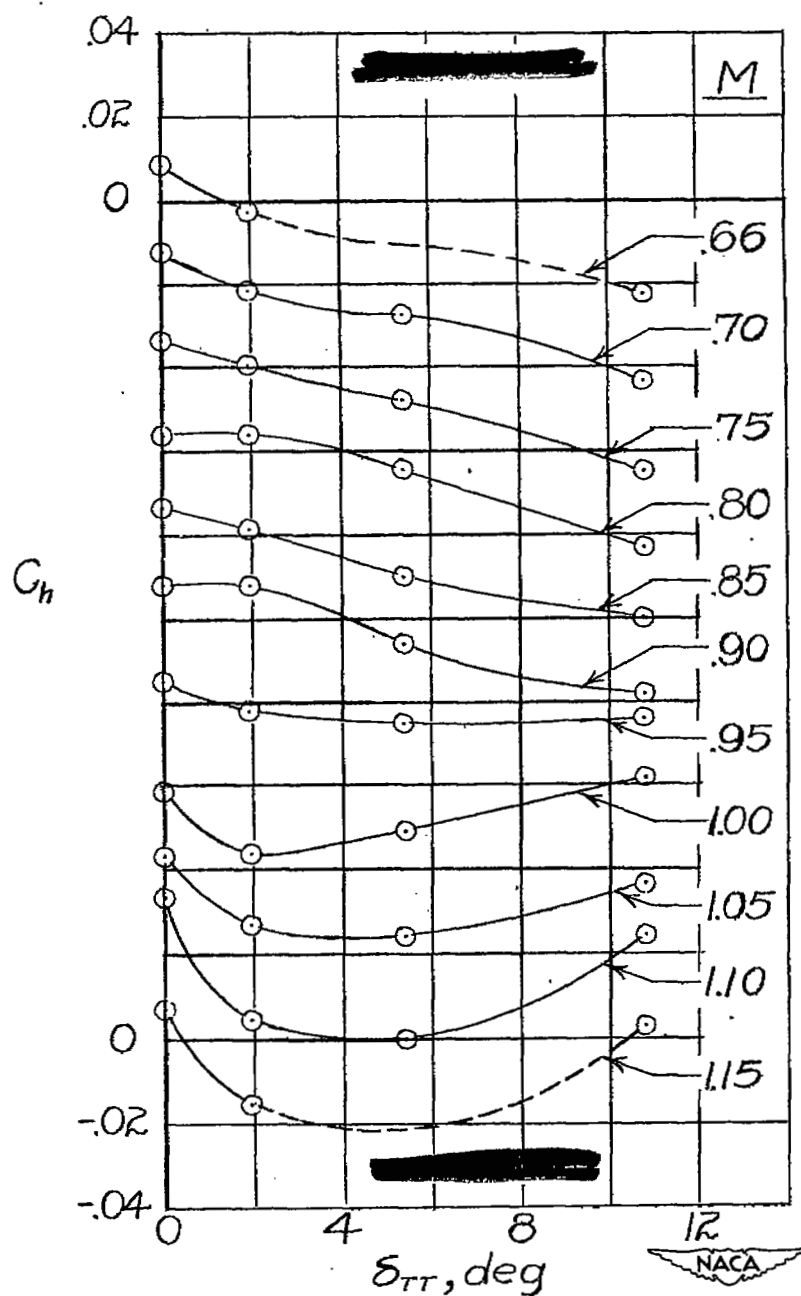


Figure 30.- Variation of hinge-moment coefficient with trim-tab deflection measured at $\alpha = 0^\circ$. NACA 65-009 airfoil, $A = 3.07$, $\Lambda = 35^\circ$, $c_f = 0.24c$, gap sealed, bevelled-trailing-edge flap, $b_{TT} = \frac{1}{3}b_f$, $\bar{c}_{TT} = \frac{1}{3}\bar{c}_f$.

